Talanta 85 (2011) 2562–2575

Contents lists available at ScienceDirect

Talanta

journal homepage: www.elsevier.com/locate/talanta

Chemical identification and determination of sulfonamides in *n*-component solid mixtures within THz-region—Solid-state Raman spectroscopic and mass spectrometric study

M. Lamshöft, B.B. Ivanova*, M. Spiteller*

Institute of Environmental Research, University of Dortmund, Otto–Hahn-Strasse 6, 44221 Dortmund, Germany

ARTICLE INFO

Article history:
Received 20 June 2011
Received in revised form 3 August 2011
Accepted 6 August 2011
Available online 12 August 2011

Keywords:
Sulfonamides
Solid-state determination and identification
Solid-mixtures
THz-regime
Raman spectroscopy
Hybrid mass spectrometry

ABSTRACT

The identification and quantitative determination of sulfonamidesin solid-state as *n*-component mixtures is performed. The limits of detection (*LODs*), accuracy, precision and repeatability are obtained and discussed, using the Raman spectra within 200–30 cm^{-1} region (6.00–0.9 THz). The excitations, corresponding to H-bonding deformations, lattice vibrations, as well as coupling modes are used for determination. The validation of the statistical and mathematical tools for procedure of the spectroscopic patterns is performed. The possibilities of baseline correction methods, smoothing procedures, and non-linear curve fitting method for quantitative analysis within THz-region for complex spectroscopic patterns of *n*-component mixtures ($n = 1–5$) are discussed. The hybrid HPLC tandem mass spectrometry (MS/MS) and powder XRD are applied as independent physical methods for analysis of the studied systems.

1. Introduction

The advantages of the THz-spectroscopy consist of the possibility for nondestructive materials identification and characterization. Thus, allowing application in interdisciplinary areas of the human, health and social science as security, environmental inspection, detection, protection, spectroscopic imaging, biomedical analysis, space communications, tomography imaging, label-free genetic analysis, and chemical/biological sensing and more. The large potential of the method for sensing and identification of chemicals is based on the fact that almost all molecules show spectral characteristics in the THz-region, related to H-bond deformations, skeletal modes, and/or lattice vibrations. Recent study drugs analysis by THz-spectroscopy has been defined the further systematic studies, relating especially the qualitative aspect of the quality control purposes. The THz-region of the electromagnetic spectrum is of great scientific fundamental interest, related the observed linear optical and nonlinear optical phenomena as well [1–22].

Therefore, the presented study aims discussion into two-fold. Firstly, to make parallel between the THz-spectroscopy and solid-state Raman method, for chemical identification. Secondly, to explore the possibility of Raman spectroscopy in a combination with mathematical methods for spectroscopic curve procedure for analysis. Especially, for the quantitative analysis, the solid-state Raman spectroscopy show remarkable for the vibrational spectroscopy *LODs* of 1.45% using the *mid*-IR region of the electromagnetic spectrum [23–31]. The application of the method within 6.0–0.9 THz need special attention, because of the lattice vibrations often are characterized with the strong intensity and well define sharp peaks, thus resulting to a possibility for quantitative application and achievement of the better LODs. The object of study is five sulfonamide drugs, characterizing with different level of the overlapping effects of the spectra within THz-region. The advantages of the applied mathematical methods are shown discussing the factors as overlapping effect, intensity, and sharp/broad character of the frequencies. The obtained results illustrate the great capability of baseline correction methods, smoothing procedures and nonlinear curve-fitting methods for study the spectroscopic patterns within THz-region. The obtained data from the non-linear methods are comparing with the classical multiple linear regression method as well as the analysis of variance for multiple linear regressions. The hybrid HPLC/mass spectrometry is used as parallel

* Corresponding authors. Tel.: +49 231 755 4080; fax: +49 231 755 40 85.
E-mail addresses: B.Ivanova@infu.tu-dortmund.de, B.Ivanova@web.de (B.B. Ivanova), Spiteller@infu.tu-dortmund.de (M. Spiteller).

0039-9140/$ – see front matter © 2011 Elsevier B.V. All rights reserved.
doi:10.1016/j.talanta.2011.08.008

independent physical method for separation and characterization of the studied solfonamides.

2. Experimental

2.1. Materials

4-Amino-N-pyridin-2-yl-benzenesulfonamide (**1**), 4-Amino-N-pyrimidin-2-yl-benzenesulfonamide (**2**), 4-Amino-N-thiazol-2-yl-benzenesulfonamide **(3)**, 4-Amino-N-(5-methyl-isoxazol-3-yl)-benzenesulfonamide (**4**) and 4-Amino-N-(3,4-dimethyl-isoxazol-5-yl)-benzenesulfonamide (**5**) were Sigma–Aldrich products.

2.2. Physical methods

Solid-state *Raman spectra* were recorded on Nicolet NXR 9610 FT-Raman spectrometer at ambient conditions (T = 298 K, P = 1 atm). HPLC–MS/MS measurements were performed, using TSQ 7000 instrument (Thermo Electron Corporation). Two mobile phase compositions were used: (A) 0.1% (v/v) aqueous HCOOH and (B) 0.1% (v/v) HCOOH in CH_3CN. Electrospray ionization (ESI) mass spectrometry. A triple quadrupole mass spectrometer (TSQ 7000 Thermo Electron, Dreieich, Germany) equipped with an ESI 2 source was used and operated at the following conditions: capillary temperature 180 °C; sheath gas 60 psi, corona 4.5 μA and spray voltage 4.5 kV. Sample was dissolved in acetonitrile (1 mg ml^{-1}) and was injected in the ion source by an autosampler (Surveyor) with a flow of pure acetonitrile (0.2 ml min^{-1}). The Excalibur 1.4 software is used. The powder X-day diffraction (XRD) measurements of polycrystalline samples were performed. The experiments prove the crystallographic space systems and groups of the studied drugs. The XRD patterns were obtained using a Rigaku MiniFlex powder diffraction system, equipped with a horizontal goniometer in the $\theta/2\theta$ mode. The X-ray source was nickel-filtered K-α emission of copper (1.5405_6 Å). Samples were packed into an aluminum holder using a back-fill procedure and will be scanned over the range of 50–6 degrees 2θ, at a scan rate of 0.5 degrees 2θ/min. Using a data acquisition rate of 1 point per second, the scanning parameters equate to a step size of 0.0084 degrees 2θ. Calibration of each powder pattern will be effected using the characteristic scattering peaks of aluminum at 44.738 and 38.472 degrees 2θ.

2.3. Statistical methods

The experimental and theoretical spectroscopic patterns were processed by R4Cal Open Office STATISTICs for Windows 7 [32] program package. Baseline corrections (BLC) and curve-fitting (CF) procedures were applied. The BLC performs operations by multipoint level or function fitting. In the multiple point level method, the baseline was leveled at a value that is the average of the baseline points. The baseline was calculated using the standard linear equation. The CF nonlinear procedure was applied. Although there are many different methods, there is no one perfect one to fit the experimental data-set. In general, non-linear peak fitting methods involve fitting a series of individual functions simultaneously, in order to obtain the single "best fit" solution. The solutions were found by iteratively trying a series of combinations of the parameters until the best one is found. Since the solutions are interdependent, small changes in one of the parameters, affect the final result of all the others. When using an iterative process, the starting point should be as close to the actual solution as possible. Good "guestimates" for the starting values increase the probability of finding the "best" solution. As always no method is perfect, and unfortunately, since there are a number of answers to a non-linear problem, many times the fit will end up in a "local minimum", which may not be the best possible solution. Many fit routines will then continue to iterate using solutions that are significantly different from the minimum, trying to find another "better" solution. If one is not found then the minimized solution is considered "best". Other problems occur if the user input values are significantly far from the "real" answer. This may end in a solution that is stuck in a local minimum that is determined to be the best fit. In extreme cases the fit may even "walk away" to a ridiculous solution. The only way to recover from this problem is to re-enter the starting fit values. Over-fitting is another common problem. Better fits can always be obtained with more input variables (given enough variables you can fit anything). Thus it is important that the input parameters reflect the proper number of variables based on the physical measurement. Using non-linear methods requires a threshold at which the "fit" is considered "good" (*i.e.* minimizing the merit equation to some near zero value). In the case of the Levenberg–Marquardt method, the merit equation used is χ^2 the equation. The final solution is found when a minimum in the reduced χ^2 equation is reached. It is a statistical measure of "goodness-of-fit", inversely proportional to the known variance of the data set. The statistical significance of each regression coefficient was checked by the use of t-test (calculation of the number of significance using data from the experimental error, usually higher than 0.100). The model fit was determined by F-test [33–51]. The most applied smoothing methods for spectroscopic curves interpretation are Savitzky–Golay (SG) and Fourier. Fourier smoothing is based on data inversion by Fast Fourier Transform (FFT) to the time domain, where a trapezoidal filter is applied to the high frequency region. Finally, an inverse FFT is applied to give the smoothed result. The degree of smoothing determines the cut-off point of the filter. A trapezoidal filter is applied to the high frequency region, then inverse FFT to give the smoothed result. The degree or percentage (%) of smoothing determines the cut-off point for the filter. SG smoothing is based on the convolution approach which performs a least-squares fit to a specified part of data points or the procedure is controlled by the level of polynomial and number of points parameters. The degree of polynomial and the number of points are controlled during the procedure by specifies the order of the polynomial to fit over the specified number of points. Thus the larger number of points specified and lower orders of polynomial heavier the smoothing. Only odd numbers are used for number of smoothing points and even values are rounded. The number of smoothing points must be one more than the "degree of polynomial" The algorithm used for generating the SG convolution coefficients has been described. It is worth mentioning that the choice of smoothing parameters is somewhat subjective data-dependent and arbitrary. The $(n-1)/2$ data points, where n is the number of points used in the convolution function, are truncated from the beginning and end of the procedure.

2.4. Quantitative analysis procedure

For the purpose of the quantitative determination are attributed the integral intensities defined as $A\nu_i^{(j,k)}$ at the ν_i frequency for the j- and k-components, common for both the analysed substances in the mixtures to the corresponding value $A\nu_i^{(j)}$ for a frequency presented in the corresponding solid-state Raman spectrum of one of the analysed compound. For the isolated compounds and the mixtures, complete separation (deconvolution) of the bands was achieved by employing the 'Peak Fit' statistical procedure, the corresponding baseline method as well as non-linear curve-fitting tools. The peak position and the area under the curve (*or* $A\nu_i^{(j)}$) of the separated frequencies were used for the qualitative chemical identification, quantitative determination as well as elucidation of the optical phenomena within the THz-region. The $A\nu_i^{(j,k)}$ is directly proportional to the reciprocal mole fraction of one of the compound ($1/X$). Repeated Raman spectroscopic analysis on three

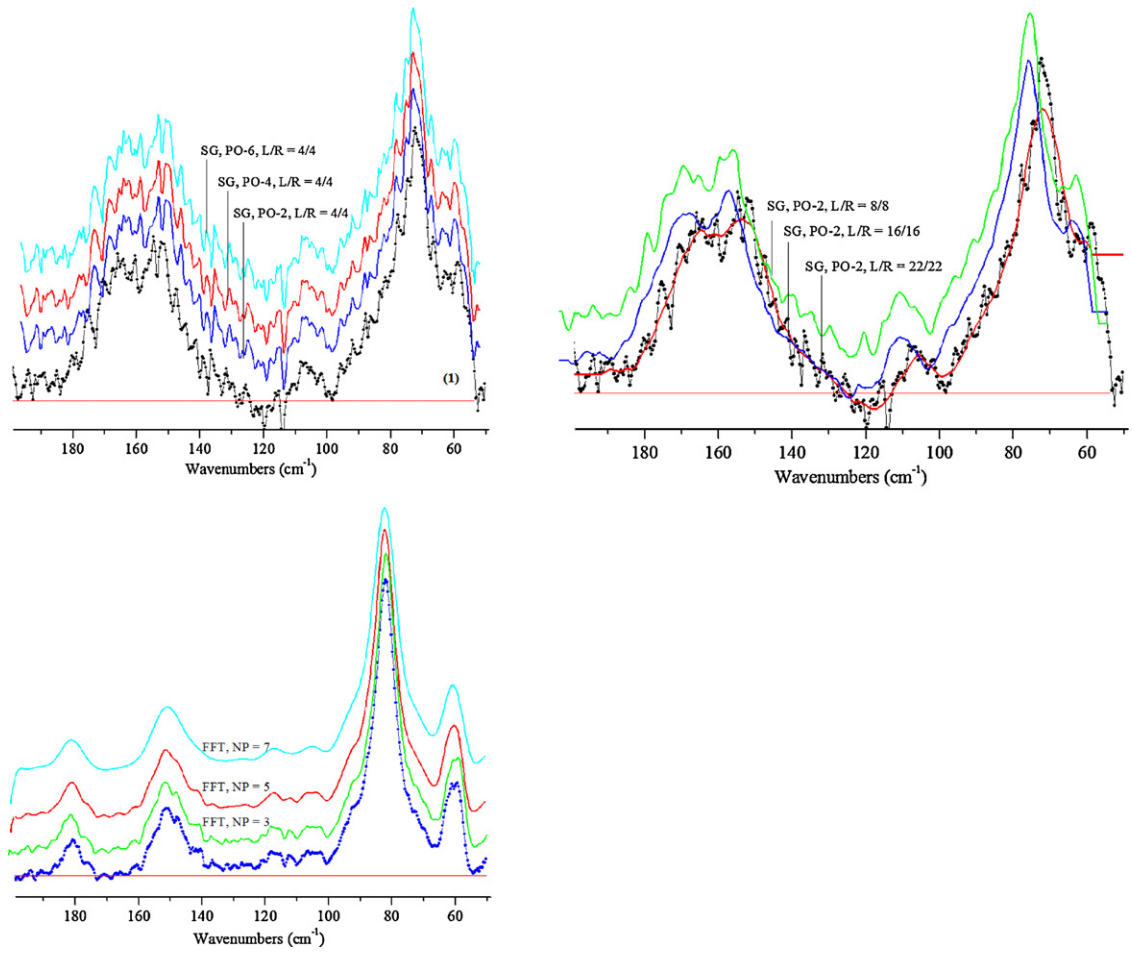

Fig. 1. Smoother solid-state Raman spectra within 200–30 cm^{-1} spectroscopic region, using Savitzki–Golay (SG) method and Fast-Fourier Transfer (FFT) filter at different number of points (NP) at left/rigth (L/R) and polynomial orders (PO); the spectroscopic patterns are preliminary procedured by the baseline correction method.

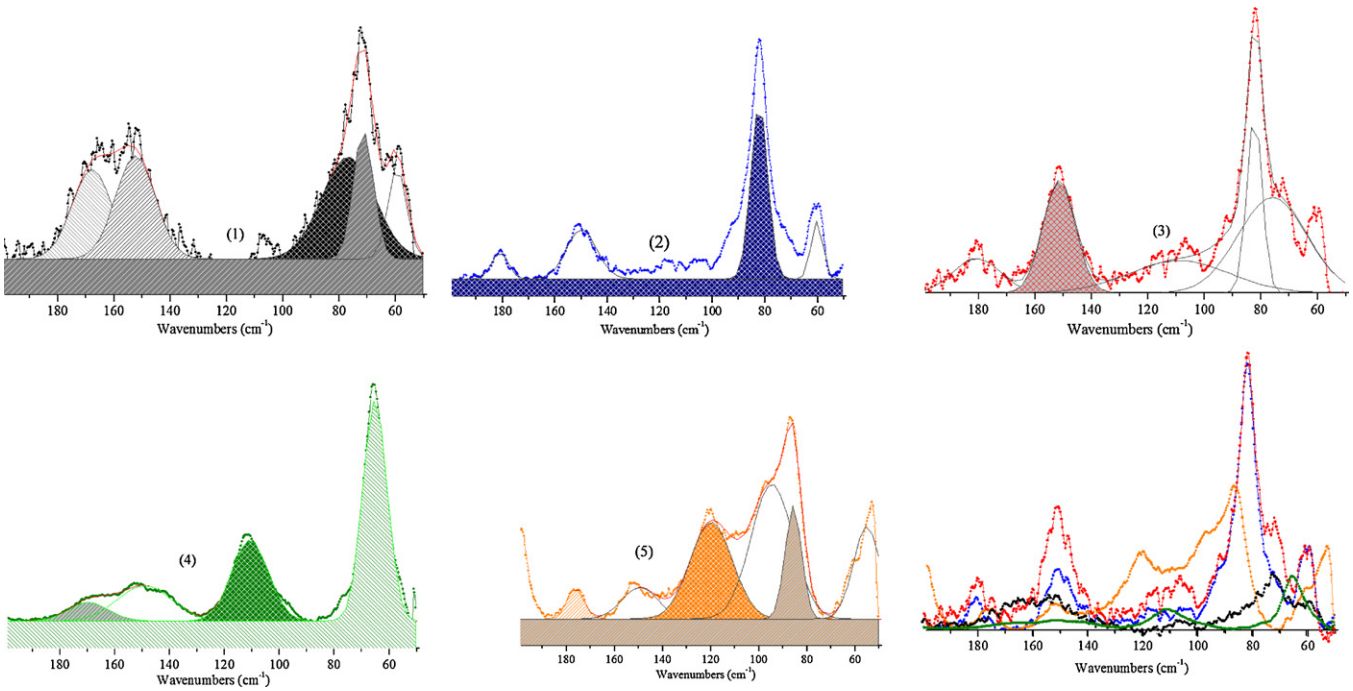

Fig. 2. Curve-fitted solid-state Raman spectra within the 200–30 cm^{-1}; curve-fitted spectroscopic patterns after the baseline correction method, by non-linear multipeak Lorenzian–Gaussian function at ratio 1:1; A is the total area under the curve from the baseline centre of the peak; w^2 "sigma", approximately 0.441 the FWHM; $w/2$ is the standard deviation, respectively.

Table 1
The experimental peak position ($\nu_i^{(j)}$) and integral intensity $A\nu_i^{(j)}$ for *i*th-peak at the Raman spectra at of the *j*-compounds **(1)**–**(5)**, obtained after the smoothing procedures, using Savitzki–Golay (SG) method and Fast-Fourier Transfor (FFT) filter at different number of points (NP) at left/rigth (L/R) and polynomial orders (PO). The obtained average values correspond to the three repeated measurements of the each of the samples.

SG-L/R	2/2		6/6		10/10		14/14		18/18		22/22		
	$\nu_i^{(j)}$	$A\nu_i^{(j)}$	$\nu_i^{(j)}$	$A\nu_i^{(j)}$	$\nu_i^{(j)}$	$A\nu_i^{(j)}$	$\nu_i^{(j)}$	$A\nu_i^{(j)}$	$\nu_i^{(j)}$	$A\nu_i^{(j)}$	$\nu_i^{(j)}$	$A\nu_i^{(j)}$	
PO-2													
$\nu_1^{(1)}$	$164.2 \pm 0.1_2$	$6.111 \pm 0.5_6$	$164.1 \pm 0.6_2$	$6.100 \pm 0.5_0$	$164.0 \pm 0.1_1$	$6.093 \pm 0.5_2$	$164.0 \pm 0.3_3$	$6.081 \pm 0.2_1$	$164.0 \pm 0.1_3$	$6.001 \pm 0.1_1$	$164.0 \pm 0.1_1$	$6.000 \pm 0.1_8$	(1)
$\nu_2^{(1)}$	$152.3 \pm 0.3_2$	$6.999 \pm 0.5_1$	$152.5 \pm 0.2_2$	$6.341 \pm 0.2_1$	$152.3 \pm 0.5_3$	$6.322 \pm 0.2_8$	$152.2 \pm 0.2_1$	$6.300 \pm 0.2_2$	$152.1 \pm 0.6_8$	$6.101 \pm 0.2_2$	$152.1 \pm 0.6_2$	$6.101 \pm 0.6_2$	
$\nu_3^{(1)}$	$72.3 \pm 0.1_5$	$9.269 \pm 0.1_7$	$72.2 \pm 0.1_3$	$9.103 \pm 0.1_3$	$72.1 \pm 0.1_1$	$9.088 \pm 0.1_1$	$72.8 \pm 0.1_3$	$9.077 \pm 0.1_0$	$72.1 \pm 0.1_2$	$9.077 \pm 0.7_0$	$72.1 \pm 0.1_7$	$9.075 \pm 0.5_0$	
$\nu_4^{(1)}$	$60.8 \pm 0.1_6$	$1.479 \pm 0.9_6$	$60.7 \pm 0.1_5$	$1.444 \pm 0.9_5$	$60.6 \pm 0.1_4$	$1.112 \pm 0.6_2$	$60.2 \pm 0.1_7$	$1.111 \pm 0.5_1$	$60.6 \pm 0.2_3$	$1.001 \pm 0.1_8$	$60.6 \pm 0.2_1$	$1.000 \pm 0.9_3$	
$\nu_1^{(2)}$	$181.5 \pm 0.0_5$	$1.221 \pm 0.5_1$	$180.3 \pm 0.1_5$	$1.210 \pm 0.3_1$	$181.4 \pm 0.1_3$	$1.209 \pm 0.1_1$	$181.5 \pm 0.5_4$	$1.200 \pm 0.0_1$	$181.3 \pm 0.6_6$	$1.199 \pm 0.4_1$	$181.2 \pm 0.1_6$	$1.220 \pm 0.2_2$	(2)
$\nu_2^{(2)}$	$153.1 \pm 0.3_2$	$4.119 \pm 0.2_3$	$153.0 \pm 0.3_7$	$4.100 \pm 0.2_0$	$153.0 \pm 0.2_5$	$4.100 \pm 0.3_9$	$153.1 \pm 0.2_1$	$4.075 \pm 0.1_3$	$153.7 \pm 0.2_9$	$4.033 \pm 0.1_3$	$153.1 \pm 0.4_7$	$4.103 \pm 0.1_8$	
$\nu_3^{(2)}$	$83.5 \pm 0.1_1$	$8.152 \pm 0.2_8$	$83.4 \pm 0.0_1$	$8.103 \pm 0.2_2$	$83.3 \pm 0.6_9$	$8.104 \pm 0.2_7$	$83.3 \pm 0.7_8$	$8.124 \pm 0.6_3$	$83.3 \pm 0.1_8$	$8.102 \pm 0.1_8$	$83.1 \pm 0.2_8$	$8.100 \pm 0.1_4$	
$\nu_4^{(2)}$	$61.2 \pm 0.2_2$	$1.967 \pm 0.3_3$	$61.1 \pm 0.1_2$	$1.944 \pm 0.1_8$	$61.1 \pm 0.1_8$	$1.955 \pm 0.3_2$	$61.1 \pm 0.5_8$	$1.955 \pm 0.2_5$	$61.1 \pm 0.3_3$	$1.955 \pm 0.1_2$	$61.2 \pm 0.1_1$	$1.902 \pm 0.0_1$	
$\nu_1^{(3)}$	$180.3 \pm 0.1_8$	$1.141 \pm 0.1_6$	$180.3 \pm 0.9_3$	$1.133 \pm 0.1_4$	$180.2 \pm 0.7_4$	$1.120 \pm 0.1_0$	$180.2 \pm 0.2_4$	$1.111 \pm 0.1_1$	$180.2 \pm 0.3_9$	$1.106 \pm 0.1_0$	$180.2 \pm 0.2_4$	$1.101 \pm 0.1_3$	(3)
$\nu_2^{(3)}$	$152.7 \pm 0.1_2$	$2.251 \pm 0.3_8$	$152.2 \pm 0.1_1$	$2.240 \pm 0.2_2$	$152.5 \pm 0.5_1$	$2.232 \pm 0.4_4$	$152.5 \pm 0.2_3$	$2.227 \pm 0.5_5$	$152.3 \pm 0.3_2$	$2.210 \pm 0.3_0$	$152.5 \pm 0.1_1$	$2.199 \pm 0.3_5$	
$\nu_3^{(3)}$	$82.8 \pm 0.1_6$	$7.166 \pm 0.3_4$	$82.0 \pm 0.3_4$	$7.150 \pm 0.2_7$	$82.5 \pm 0.1_3$	$7.155 \pm 0.2_2$	$82.4 \pm 0.1_0$	$7.140 \pm 0.2_3$	$82.9 \pm 0.1_0$	$7.133 \pm 0.7_8$	$82.2 \pm 0.1_1$	$7.127 \pm 0.3_2$	
$\nu_1^{(4)}$	$110.3 \pm 0.5_8$	$4.886 \pm 0.6_2$	$110.2 \pm 0.5_3$	$4.833 \pm 0.1_7$	$110.2 \pm 0.3_2$	$4.813 \pm 0.2_2$	$110.1 \pm 0.3_1$	$4.810 \pm 0.6_2$	$110.3 \pm 0.5_8$	$4.808 \pm 0.1_4$	$110.2 \pm 0.5_1$	$4.800 \pm 0.2_1$	(4)
$\nu_2^{(4)}$	$64.2 \pm 0.6_6$	$8.867 \pm 0.2_5$	$64.1 \pm 0.6_3$	$8.850 \pm 0.1_3$	$64.1 \pm 0.3_2$	$8.842 \pm 0.1_2$	$64.1 \pm 0.5_5$	$8.807 \pm 0.2_5$	$64.2 \pm 0.6_6$	$8.800 \pm 0.1_2$	$64.1 \pm 0.6_2$	$8.844 \pm 0.1_2$	
$\nu_1^{(5)}$	$177.4 \pm 0.4_3$	$0.993 \pm 0.3_2$	$177.2 \pm 0.1_2$	$0.966 \pm 0.2_1$	$177.2 \pm 0.1_7$	$0.948 \pm 0.2_1$	$177.2 \pm 0.5_2$	$0.953 \pm 0.3_2$	$177.4 \pm 0.4_3$	$0.950 \pm 0.2_2$	$177.2 \pm 0.4_2$	$0.949 \pm 0.1_2$	(5)
$\nu_2^{(5)}$	$120.1 \pm 0.5_1$	$2.170 \pm 0.5_5$	$120.0 \pm 0.5_0$	$2.150 \pm 0.1_2$	$120.0 \pm 0.3_3$	$2.133 \pm 0.1_2$	$120.0 \pm 0.4_2$	$2.130 \pm 0.5_5$	$120.1 \pm 0.5_1$	$2.120 \pm 0.5_5$	$120.3 \pm 0.5_2$	$2.118 \pm 0.5_5$	
$\nu_3^{(5)}$	$87.1 \pm 0.7_8$	$7.939 \pm 0.1_8$	$87.0 \pm 0.7_5$	$7.933 \pm 0.0_3$	$87.0 \pm 0.6_6$	$7.912 \pm 0.0_9$	$87.0 \pm 0.7_5$	$7.909 \pm 0.1_8$	$87.1 \pm 0.7_8$	$7.900 \pm 0.1_1$	$87.1 \pm 0.7_5$	$7.900 \pm 0.1_8$	
SG-PO-4													
$\nu_1^{(1)}$	$164.2 \pm 0.1_2$	$6.111 \pm 0.4_2$	$164.0 \pm 0.3_2$	$6.092 \pm 0.5_1$	$164.0 \pm 0.3_5$	$6.088 \pm 0.1_4$	$164.0 \pm 0.6_2$	$6.070 \pm 0.2_0$	$164.0 \pm 0.3_7$	$6.000 \pm 0.2_1$	$164.0 \pm 0.0_0$	$5.982 \pm 0.1_3$	(1)
$\nu_2^{(1)}$	$152.3 \pm 0.3_1$	$6.999 \pm 0.1_2$	$152.2 \pm 0.2_1$	$6.333 \pm 0.2_0$	$152.3 \pm 0.5_4$	$6.310 \pm 0.1_7$	$152.2 \pm 0.1_3$	$6.289 \pm 0.2_0$	$152.1 \pm 0.9_2$	$6.088 \pm 0.3_2$	$152.1 \pm 0.2_1$	$5.943 \pm 0.7_1$	
$\nu_3^{(1)}$	$72.3 \pm 0.2_5$	$9.268 \pm 0.1_2$	$72.2 \pm 0.1_2$	$9.100 \pm 0.1_1$	$72.1 \pm 0.4_1$	$9.088 \pm 0.2_3$	$72.8 \pm 0.3_6$	$9.052 \pm 0.2_0$	$72.1 \pm 0.2_7$	$9.052 \pm 0.7_0$	$72.1 \pm 0.3_5$	$9.011 \pm 0.5_2$	
$\nu_4^{(1)}$	$60.8 \pm 0.1_2$	$1.479 \pm 0.5_6$	$60.5 \pm 0.1_2$	$1.411 \pm 0.9_0$	$60.6 \pm 0.2_3$	$1.102 \pm 0.5_2$	$60.2 \pm 0.2_7$	$1.092 \pm 0.3_1$	$60.6 \pm 0.1_9$	$1.000 \pm 0.2_8$	$60.6 \pm 0.1_1$	$0.993 \pm 0.2_3$	
$\nu_1^{(2)}$	$181.5 \pm 0.0_1$	$1.220 \pm 0.5_1$	$180.3 \pm 0.1_5$	$1.209 \pm 0.3_3$	$181.4 \pm 0.2_8$	$1.207 \pm 0.0_1$	$181.5 \pm 0.9_1$	$1.199 \pm 0.1_1$	$181.3 \pm 0.7_1$	$1.169 \pm 0.5_0$	$181.2 \pm 0.5_8$	$1.218 \pm 0.2_1$	(2)
$\nu_2^{(2)}$	$153.1 \pm 0.3_0$	$4.119 \pm 0.2_2$	$153.0 \pm 0.1_2$	$4.092 \pm 0.2_1$	$153.0 \pm 0.2_9$	$4.099 \pm 0.2_3$	$153.1 \pm 0.5_2$	$4.062 \pm 0.3_3$	$153.7 \pm 0.3_5$	$4.024 \pm 0.2_3$	$153.1 \pm 0.9_1$	$4.077 \pm 0.1_2$	
$\nu_3^{(2)}$	$83.5 \pm 0.1_6$	$8.151 \pm 0.2_7$	$83.4 \pm 0.5_3$	$8.096 \pm 0.2_5$	$83.3 \pm 0.3_1$	$8.100 \pm 0.2_2$	$83.3 \pm 0.9_3$	$8.122 \pm 0.6_3$	$83.3 \pm 0.9_3$	$8.097 \pm 0.2_2$	$83.1 \pm 0.3_1$	$8.042 \pm 0.1_1$	
$\nu_4^{(2)}$	$61.2 \pm 0.2_1$	$1.966 \pm 0.3_2$	$61.1 \pm 0.2_2$	$1.943 \pm 0.1_2$	$61.1 \pm 0.2_3$	$1.933 \pm 0.2_1$	$61.1 \pm 0.9_1$	$1.940 \pm 0.2_4$	$61.1 \pm 0.3_7$	$1.933 \pm 0.2_2$	$61.2 \pm 0.7_6$	$1.702 \pm 0.0_2$	
$\nu_1^{(3)}$	$180.3 \pm 0.1_2$	$1.140 \pm 0.1_6$	$180.3 \pm 0.5_8$	$1.142 \pm 0.1_6$	$180.3 \pm 0.5_4$	$1.139 \pm 0.1_5$	$180.3 \pm 0.7_2$	$1.140 \pm 0.1_5$	$180.3 \pm 0.2_9$	$1.137 \pm 0.1_5$	$180.3 \pm 0.9_6$	$1.121 \pm 0.1_7$	(3)
$\nu_2^{(3)}$	$152.7 \pm 0.1_2$	$2.250 \pm 0.3_6$	$152.7 \pm 0.1_2$	$2.250 \pm 0.3_5$	$152.7 \pm 0.3_6$	$2.245 \pm 0.2_3$	$152.7 \pm 0.6_8$	$2.241 \pm 0.3_2$	$152.7 \pm 0.1_1$	$2.244 \pm 0.3_3$	$152.7 \pm 0.8_1$	$2.231 \pm 0.3_1$	
$\nu_3^{(3)}$	$82.8 \pm 0.1_1$	$7.166 \pm 0.3_3$	$82.8 \pm 0.1_2$	$7.144 \pm 0.1_4$	$82.8 \pm 0.2_4$	$7.155 \pm 0.3_1$	$82.8 \pm 0.9_2$	$7.150 \pm 0.3_4$	$82.8 \pm 0.1_4$	$7.150 \pm 0.3_3$	$82.8 \pm 0.2_6$	$7.155 \pm 0.3_1$	
$\nu_1^{(4)}$	$110.3 \pm 0.4_8$	$4.885 \pm 0.6_2$	$110.3 \pm 0.5_1$	$4.877 \pm 0.5_2$	$110.3 \pm 0.1_2$	$4.875 \pm 0.2_3$	$110.3 \pm 0.8_3$	$4.879 \pm 0.5_1$	$110.3 \pm 0.5_1$	$4.877 \pm 0.4_2$	$110.3 \pm 0.5_1$	$4.865 \pm 0.2_2$	(4)
$\nu_2^{(4)}$	$64.2 \pm 0.5_5$	$8.868 \pm 0.2_5$	$64.2 \pm 0.7_8$	$8.851 \pm 0.2_1$	$64.2 \pm 0.6_8$	$8.866 \pm 0.1_5$	$64.2 \pm 0.7_8$	$8.860 \pm 0.2_1$	$64.2 \pm 0.1_7$	$8.859 \pm 0.2_1$	$64.2 \pm 0.6_2$	$8.839 \pm 0.2_1$	
$\nu_1^{(5)}$	$177.4 \pm 0.5_2$	$0.992 \pm 0.3_2$	$177.4 \pm 0.5_1$	$0.966 \pm 0.3_1$	$177.4 \pm 0.7_7$	$0.991 \pm 0.3_1$	$177.4 \pm 0.4_2$	$0.990 \pm 0.3_3$	$177.4 \pm 0.5_2$	$0.977 \pm 0.2_2$	$177.4 \pm 0.5_3$	$0.982 \pm 0.2_2$	(5)
$\nu_2^{(5)}$	$120.1 \pm 0.5_1$	$2.171 \pm 0.5_1$	$120.1 \pm 0.2_2$	$2.169 \pm 0.1_1$	$120.1 \pm 0.5_9$	$2.166 \pm 0.5_0$	$120.1 \pm 0.5_0$	$2.163 \pm 0.5_1$	$120.1 \pm 0.5_5$	$2.169 \pm 0.5_2$	$120.1 \pm 0.5_7$	$2.179 \pm 0.1_5$	
$\nu_3^{(5)}$	$87.1 \pm 0.7_1$	$7.938 \pm 0.1_3$	$87.1 \pm 0.9_2$	$7.928 \pm 0.1_2$	$87.1 \pm 0.6_3$	$7.925 \pm 0.1_1$	$87.1 \pm 0.7_1$	$7.933 \pm 0.1_2$	$87.1 \pm 0.8_8$	$7.955 \pm 0.1_1$	$87.1 \pm 0.8_8$	$7.918 \pm 0.1_2$	
SG-PO-6													
$\nu_1^{(1)}$	$164.2 \pm 0.2_1$	$6.110 \pm 0.5_3$	$164.1 \pm 0.4_3$	$6.097 \pm 0.2_0$	$164.0 \pm 0.1_5$	$6.001 \pm 0.5_2$	$164.0 \pm 0.1_3$	$6.055 \pm 0.2_2$	$164.0 \pm 0.1_1$	$5.997 \pm 0.2_1$	$164.0 \pm 0.1_2$	$5.994 \pm 0.2_8$	(1)
$\nu_2^{(1)}$	$152.3 \pm 0.1_2$	$6.977 \pm 0.5_0$	$152.5 \pm 0.3_2$	$6.322 \pm 0.2_1$	$152.3 \pm 0.5_1$	$6.112 \pm 0.2_3$	$152.2 \pm 0.1_7$	$6.220 \pm 0.2_1$	$152.1 \pm 0.6_2$	$6.055 \pm 0.2_2$	$152.1 \pm 0.6_3$	$6.000 \pm 0.5_2$	
$\nu_3^{(1)}$	$72.3 \pm 0.1_2$	$9.267 \pm 0.1_8$	$72.2 \pm 0.1_8$	$9.100 \pm 0.1_1$	$72.1 \pm 0.2_3$	$9.025 \pm 0.1_7$	$72.8 \pm 0.9_2$	$9.068 \pm 0.0_0$	$72.1 \pm 0.1_2$	$9.031 \pm 0.6_0$	$72.1 \pm 0.1_2$	$9.055 \pm 0.3_0$	
$\nu_4^{(1)}$	$60.8 \pm 0.12_6$	$1.478 \pm 0.9_2$	$60.7 \pm 0.1_9$	$1.427 \pm 0.3_5$	$60.6 \pm 0.3_4$	$1.102 \pm 0.6_3$	$60.2 \pm \pm 0.3_5$	$1.100 \pm 0.5_5$	$60.6 \pm 0.2_3$	$1.000 \pm 0.1_2$	$60.6 \pm 0.2_7$	$0.971 \pm 0.8_3$	
$\nu_1^{(2)}$	$181.5 \pm 0.1_5$	$1.220 \pm 0.3_1$	$180.3 \pm 0.2_5$	$1.201 \pm 0.1_1$	$181.4 \pm 0.1_1$	$1.200 \pm 0.1_0$	$181.5 \pm 0.5_1$	$1.177 \pm 0.2_1$	$181.3 \pm 0.6_1$	$1.177 \pm 0.6_1$	$181.2 \pm 0.3_6$	$1.188 \pm 0.2_2$	(2)
$\nu_2^{(2)}$	$153.1 \pm 0.2_2$	$4.118 \pm 0.1_3$	$153.0 \pm 0.8_7$	$3.999 \pm 0.1_0$	$153.0 \pm 0.8_2$	$4.100 \pm 0.3_2$	$153.1 \pm 0.2_0$	$4.043 \pm 0.1_2$	$153.7 \pm 0.3_1$	$4.021 \pm 0.1_3$	$153.1 \pm 0.4_1$	$4.001 \pm 0.2_8$	
$\nu_3^{(2)}$	$83.5 \pm 0.2_1$	$8.151 \pm 0.2_1$	$83.4 \pm 0.0_8$	$8.103 \pm 0.2_2$	$83.3 \pm 0.9_1$	$8.100 \pm 0.2_1$	$83.3 \pm 0.7_1$	$8.115 \pm 0.6_3$	$83.3 \pm 0.2_3$	$8.005 \pm 0.1_9$	$83.1 \pm 0.3_2$	$8.093 \pm 0.4_4$	
$\nu_4^{(2)}$	$61.2 \pm 0.2_1$	$1.968 \pm 0.3_3$	$61.1 \pm 0.1_9$	$1.944 \pm 0.1_8$	$61.1 \pm 0.3_2$	$1.913 \pm 0.3_2$	$61.1 \pm 0.6_2$	$1.944 \pm 0.2_1$	$61.1 \pm 0.1_8$	$1.933 \pm 0.1_1$	$61.2 \pm 0.1_3$	$1.900 \pm 0.0_0$	
$\nu_1^{(3)}$	$180.3 \pm 0.1_1$	$1.140 \pm 0.1_6$	$180.3 \pm 0.2_8$	$1.141 \pm 0.1_6$	$180.3 \pm 0.9_1$	$1.128 \pm 0.1_3$	$180.3 \pm 0.8_1$	$1.135 \pm 0.1_7$	$180.3 \pm 0.9_1$	$1.127 \pm 0.1_2$	$180.3 \pm 0.7_1$	$1.133 \pm 0.1_2$	(3)
$\nu_2^{(3)}$	$152.7 \pm 0.1_2$	$2.250 \pm 0.3_8$	$152.7 \pm 0.1_7$	$2.251 \pm 0.3_8$	$152.7 \pm 0.5_2$	$2.244 \pm 0.3_5$	$152.7 \pm 0.9_2$	$2.250 \pm 0.3_1$	$152.7 \pm 0.3_1$	$2.227 \pm 0.3_1$	$152.7 \pm 0.1_2$	$2.250 \pm 0.3_3$	
$\nu_3^{(3)}$	$82.8 \pm 0.1_2$	$7.161 \pm 0.3_4$	$82.8 \pm 0.2_7$	$7.166 \pm 0.3_4$	$82.8 \pm 0.7_1$	$7.155 \pm 0.3_1$	$82.8 \pm 0.1_2$	$7.144 \pm 0.3_4$	$82.8 \pm 0.7_1$	$7.144 \pm 0.3_1$	$82.8 \pm 0.3_6$	$7.152 \pm 0.3_5$	
$\nu_1^{(4)}$	$110.3 \pm 0.5_6$	$4.885 \pm 0.6_2$	$110.3 \pm 0.1_9$	$4.886 \pm \pm 0.6_2$	$110.3 \pm 0.9_1$	$4.833 \pm 0.6_2$	$110.3 \pm 0.4_1$	$4.871 \pm 0.6_1$	$110.3 \pm 0.5_8$	$4.873 \pm 0.6_1$	$110.3 \pm 0.1_8$	$4.866 \pm 0.5_3$	(4)
$\nu_2^{(4)}$	$64.2 \pm 0.6_8$	$8.866 \pm 0.2_5$	$64.2 \pm 0.5_8$	$8.867 \pm 0.2_5$	$64.2 \pm 0.7_1$	$8.855 \pm 0.2_1$	$64.2 \pm 0.2_6$	$8.832 \pm 0.2_1$	$64.2 \pm 0.6_5$	$8.882 \pm 0.1_5$	$64.2 \pm 0.6_6$	$8.893 \pm 0.2_1$	
$\nu_1^{(5)}$	$177.4 \pm 0.4_9$	$0.992 \pm 0.3_1$	$177.4 \pm 0.2_3$	$0.993 \pm \pm 0.3_2$	$177.4 \pm 0.7_1$	$0.918 \pm 0.3_1$	$177.4 \pm 0.4_1$	$0.919 \pm 0.1_2$	$177.4 \pm 0.5_5$	$0.944 \pm 0.2_2$	$177.4 \pm 0.6_3$	$0.933 \pm 0.4_1$	(5)
$\nu_2^{(5)}$	$120.1 \pm 0.5_3$	$2.171 \pm 0.5_5$	$120.1 \pm 0.1_1$	$2.170 \pm 0.5_5$	$120.1 \pm 0.9_1$	$2.155 \pm 0.5_1$	$120.1 \pm 0.5_0$	$2.152 \pm 0.1_5$	$120.1 \pm 0.5_5$	$2.166 \pm 0.1_5$	$120.1 \pm 0.5_7$	$2.149 \pm 0.1_9$	
$\nu_3^{(5)}$	$87.1 \pm 0.7_2$	$7.937 \pm 0.1_8$	$87.1 \pm 0.7_9$	$7.939 \pm \pm 0.1_8$	$87.1 \pm 0.9_8$	$7.927 \pm 0.1_1$	$87.1 \pm 0.7_3$	$7.929 \pm 0.2_8$	$87.1 \pm 0.7_5$	$7.919 \pm 0.2_8$	$87.1 \pm 0.7_9$	$7.911 \pm 0.2_7$	

Table 1 (*Continued*)

SG-L/R	2/2		6/6		10/10		14/14		18/18		22/22		
	$\nu_i^{(j)}$	$A\nu_i^{(j)}$	$\nu_i^{(j)}$	$A\nu_i^{(j)}$	$\nu_i^{(j)}$	$A\nu_i^{(j)}$	$\nu_i^{(j)}$	$A\nu_i^{(j)}$	$\nu_i^{(j)}$	$A\nu_i^{(j)}$	$\nu_i^{(j)}$	$A\nu_i^{(j)}$	
FFT-NP	3		5		7		9						
$\nu_1^{(1)}$	$164.2 \pm 0.2_2$	$6.110 \pm 0.5_2$	$164.1 \pm 0.6_3$	$6.057 \pm 0.5_1$	$164.0 \pm 0.2_1$	$6.064 \pm 0.5_1$	$164.0 \pm 0.2_2$	$6.033 \pm 0.2_3$					(1)
$\nu_2^{(1)}$	$152.3 \pm 0.4_2$	$6.986 \pm 0.5_0$	$152.5 \pm 0.3_3$	$6.243 \pm 0.1_1$	$152.3 \pm 0.2_3$	$6.310 \pm 0.2_1$	$152.2 \pm 0.1_7$	$6.271 \pm 0.1_2$					
$\nu_3^{(1)}$	$72.3 \pm 0.2_5$	$9.266 \pm 0.1_2$	$72.2 \pm 0.3_9$	$9.005 \pm 0.0_2$	$72.1 \pm 0.3_1$	$9.073 \pm 0.1_9$	$72.8 \pm 0.6_1$	$9.034 \pm 0.2_0$					
$\nu_4^{(1)}$	$60.8 \pm 0.2_6$	$1.475 \pm 0.9_1$	$60.7 \pm 0.4_7$	$1.430 \pm 0.8_8$	$60.3 \pm 0.1_8$	$1.018 \pm 0.6_2$	$60.2 \pm 0.8_2$	$1.056 \pm 0.5_2$					
$\nu_1^{(2)}$	$181.5 \pm 0.0_2$	$1.220 \pm 0.5_0$	$180.3 \pm 0.8_2$	$1.200 \pm 0.2_1$	$181.4 \pm 0.9_3$	$1.200 \pm 0.2_1$	$181.5 \pm 0.7_2$	$1.188 \pm 0.1_1$					(2)
$\nu_2^{(2)}$	$153.1 \pm 0.1_2$	$4.117 \pm 0.1_2$	$153.0 \pm 0.4_7$	$4.082 \pm 0.2_0$	$153.0 \pm 0.9_1$	$4.092 \pm 0.3_1$	$153.1 \pm 0.9_1$	$4.055 \pm 0.3_3$					
$\nu_3^{(2)}$	$83.5 \pm 0.1_8$	$8.151 \pm 0.2_4$	$83.4 \pm 0.5_1$	$8.033 \pm 0.3_2$	$83.3 \pm 0.7_2$	$8.087 \pm 0.2_2$	$83.3 \pm 0.8_9$	$8.115 \pm 0.3_3$					
$\nu_4^{(2)}$	$61.2 \pm 0.2_2$	$1.965 \pm 0.3_1$	$61.1 \pm 0.8_2$	$1.930 \pm 0.1_8$	$61.1 \pm 0.3_1$	$1.933 \pm 0.3_1$	$61.1 \pm 0.5_1$	$1.905 \pm 0.1_5$					
$\nu_1^{(3)}$	$180.3 \pm 0.1_8$	$1.141 \pm 0.1_6$	$180.3 \pm 0.9_2$	$1.140 \pm 0.2_3$	$180.3 \pm 0.9_2$	$1.128 \pm 0.1_2$	$180.3 \pm 0.5_8$	$1.139 \pm 0.2_6$					(3)
$\nu_2^{(3)}$	$152.7 \pm 0.1_4$	$2.250 \pm 0.3_6$	$152.7 \pm 0.8_2$	$2.250 \pm 0.5_2$	$152.7 \pm 0.1_8$	$2.242 \pm 0.3_3$	$152.7 \pm 0.5_2$	$2.222 \pm 0.1_8$					
$\nu_3^{(3)}$	$82.8 \pm 0.1_2$	$7.165 \pm 0.3_5$	$82.8 \pm 0.7_6$	$7.122 \pm 0.8_9$	$82.8 \pm 0.9_1$	$7.155 \pm 0.3_2$	$82.8 \pm 0.4_4$	$7.155 \pm 0.1_4$					
$\nu_1^{(4)}$	$110.3 \pm 0.5_2$	$4.885 \pm 0.6_1$	$110.3 \pm 0.6_8$	$4.877 \pm 0.5_2$	$110.3 \pm 0.9_1$	$4.877 \pm 0.6_2$	$110.3 \pm 0.1_8$	$4.816 \pm 0.1_2$					(4)
$\nu_2^{(4)}$	$64.2 \pm 0.6_1$	$8.864 \pm 0.2_1$	$64.2 \pm 0.5_6$	$8.854 \pm 0.1_5$	$64.2 \pm 0.6_1$	$8.855 \pm 0.2_1$	$64.2 \pm 0.5_5$	$8.855 \pm 0.1_5$					
$\nu_1^{(5)}$	$177.4 \pm 0.4_8$	$0.991 \pm 0.1_2$	$177.4 \pm 0.1_3$	$0.922 \pm 0.2_2$	$177.4 \pm 0.5_9$	$0.955 \pm 0.3_1$	$177.4 \pm 0.5_3$	$0.977 \pm 0.3_3$					(5)
$\nu_2^{(5)}$	$120.1 \pm 0.4_1$	$2.169 \pm 0.2_5$	$120.1 \pm 0.2_1$	$2.169 \pm 0.8_5$	$120.1 \pm 0.5_9$	$2.156 \pm 0.5_1$	$120.1 \pm 0.1_1$	$2.161 \pm 0.1_5$					
$\nu_3^{(5)}$	$87.1 \pm 0.6_8$	$7.929 \pm 0.1_1$	$87.1 \pm 0.2_8$	$7.929 \pm 0.1_8$	$87.1 \pm 0.7_0$	$7.929 \pm 0.1_8$	$87.1 \pm 0.7_1$	$7.927 \pm 0.1_7$					

replicate samples for each mole fraction was applied as well as the measurements is repeated three times. The results of mean value for area ratio of the peaks together with between assay precision data (RSD%) are presented. Regression analysis of the data gave a straight-line calibration plot with confidence intervals for slope and intercept, are defined. The validity of the obtained equations is confirmed from the spectrum of the pure substances where the corresponding $A\nu_i^{(j)}/A\nu_i^{(k)}$ values are obtained. The $A\nu_i^{(j)}$ measured in the Raman spectrum depends on the intensity of the laser I_o, on a factor $K(\nu_i)$ including the frequency dependent terms (such as overall spectrophotometer response, self-absorption of the medium and molecular scattering of the Raman active species), and on the mole fraction (X) of the active species. Therefore, for two component mixtures, the equations are:

$$A\nu_i^{(j)} = I_o K(\nu_i^{(j)})X$$

Therefore, $A\nu_i^{(j,k)}/A\nu_i^{(j)} = [K^{(j)}\nu_i^{(j,k)}X + K^{(k)}\nu_i^{(k)}(1-X)]/K^{(j)}\nu_i^{(j,k)}X$.

2.5. Multiple linear regression (MLR)

To perform a MLR analysis on the data, highlight the independent variable columns of data sets. The first group contains the dependent variable values, Y, and the highlighted columns assumed to contain the independent variables, X. The common statement consists of that the dependent data, y_i, depends linearly on several independent variables, $x_1, x_2, \ldots, x_k$ as well as that the given data depends only on two independent variables. The data sets could be written as $(x_{11}, x_{21}, y_1), (x_{12}, x_{22}, y_2), (x_{13}, x_{23}, y_3), \ldots, (x_{1N}, x_{2N}, y_N)$, respectively. The main aim is to minimize the sum:

$$R^2 = \sum_{i=1}^{N} (a_1 x_{1i} + a_2 x_{2i} + b - y_i)^2$$

The corresponding coefficients a_0, a_1, a_2 so are found by the following equations:

$$a_1 x_{11} + a_2 x_{21} + b = y_1$$
$$a_1 x_{12} + a_2 x_{22} + b = y_2$$
$$a_1 x_{13} + a_2 x_{23} + b = y_3$$
$$\ldots$$
$$a_1 x_{1N} + a_2 x_{2N} + b = y_N$$

In matrix form the following presentation is valid: $A \cdot W = Y$

$$A = \begin{pmatrix} x_{11} & x_{21} & 1 \\ x_{12} & x_{22} & 1 \\ x_{1N} & x_{2N} & 1 \end{pmatrix}; \quad W = \begin{pmatrix} a_1 \\ a_2 \\ b \end{pmatrix} \quad \text{and} \quad Y = \begin{pmatrix} y_1 \\ y_2 \\ y_N \end{pmatrix}$$

The solution of this predetermined system is $W = (A^t A)^{-1} A^t Y$

The obtained values are respectively, t-value: The t-values for testing if the parameter equals zero, where t = the parameter estimate/standard error of the estimate; p-value: The corresponding p-values. A partial F-test is computed for each of the independent variables still in the equation. F statistic = $[RSS^2 - RSS^1]/ESD^2$, where RSS^1 = the residual sum of squares with all variables that are presently in the equation; RSS^2 = the residual sum of squares with one of the variables removed, and ESD^1 = the Mean Square for Error with all variables that are presently in the equation [52–54].

2.6. Analysis of variance (ANOVA) for MLR

The ANOVA test includes Levene's test and the Brown–Forsythe test for equal variance. It is preformed to test whether or not two or

Table 2
Solid-state Raman frequencies and assignment of the studied compounds within 200–30 cm^{-1}; ν [cm^{-1} (THz)].

	(1)	(2)	(3)	(4)	(5)
H-bonding deformations NH···O(SO), NH···N_{Py}		181 (5.4_3)	180 (5.4)	170 (5.1)	177 (5.3_1)
	164 (4.9_2)				
	152 (4.5_6)	153 (4.5_9)	157 (4.7_1)	157 (4.7_1)/144 (4.3_2)	153 (4.5_9)
					120 (3.6)
		111 (3.3_3)	110 (3.3)	110 (3.3)	
Skeletal modes	103 (3.0_9)				98 (2.9_4)
		83 (2.4_9)	85 (2.5_5)		87 (2.6_1)
	72 (2.1_6)		71 (2.1_3)		
	60 (1.8)	61 (1.8_3)	62 (1.8_6)	64 (1.9_2)	60 (1.8)
Torsion of entire side chain about the aromatic system					55 (1.6_5)

Table 3
Student's *t*-test data for the smoothed by Savitzky–Golay and Fourier methods; $N = 16$.

SG-L/R					SG-L/R				
PO-2	r	r^2	SD	p	PO-4	r	r^2	SD	p
2/2–6/6	0.9941_2	0.9882_7	0.533	<0.0001	2/2–6/6	0.9922_1	0.9824_9	0.667	<0.0001
2/2–10/10	0.9911_2	0.9823_1	0.432	0.0421	2/2–10/10	0.9831_2	0.9665_2	0.731	0.2521
2/2–22/22	0.9901_3	0.9803_5	0.762	0.0720	2/2–22/22	0.9901	0.9802_9	0.785	0.1217

SG-L/R					SG-FFT				
PO-6	r	r^2	SD	p		r	r^2	SD	p
2/2–6/6	0.9921_1	0.9842_8	0.531	<0.0001	PO-2 L/R 10/10, NP-3	0.9998	0.9996	0.427	<0.0001
2/2–10/10	0.9909_3	0.9819_4	0.312	0.0121					
2/2–22/22	0.9902_1	0.9805_1	0.352	0.0220					

Table 4
The straight-line plot from the regression analysis of the *n*-component mixtures; $y = A + B{\cdot}x$; $N = 10$.

	A	B	SD	r^2	p
(3)/(4)	11.0 ± 0.034	−1.0 ± 0.21	0.003	0.9998_9	<0.0001
(2)/(5)	2.905 ± 0.066	−0.174 ± 0.21	0.088	0.9876_2	<0.0001
(1)/(4)	1.789 ± 0.071	−0.095 ± 0.011	0.105	0.9461	<0.0001
(2)/(3)/(4)–(4)	3.069 ± 0.038	−0.121 ± 0.006	0.057	0.9894_2	<0.0001
(2)/(3)/(4)–(3)	1.913 ± 0.405	1.493 ± 0.065	0.593	0.9924_3	<0.0001
(1)/(3)/(4)/(5)–(3)	0.516 ± 0.005	0.024 ± 0.000	0.008	0.9949_1	<0.0001
(1)/(2)/(3)/(4)–(3)/(2)	0.883 ± 0.011	0.038 ± 0.002	0.016	0.9917_5	<0.0001
(1)/(2)/(3)/(4)/(5)–(3)/(2)	0.939 ± 0.014	−0.041 ± 0.002	0.0204	0.9884_3	<0.0001
(1)/(2)/(3)/(4)/(5)–(5)	14.141 ± 0.135	−1.103 ± 0.022	0.198	0.9984_4	<0.0001

more populations have the same mean. The main analysis is based on the assumption that the data sets have been drawn from populations that follow a normal distribution with constant variance. The null hypothesis is that the means of all selected data sets are equal. The alternative hypothesis is that the means of one or more selected data sets are different [55,56].

The basic equations for the ANOVA calculations are:

$$(y_i - \bar{y}) = (\hat{y}_i - \bar{y}) + (y_i - \hat{y}_i)$$

The first term is the total variation, while the second term is the variation in mean response. The third term is the residual value. The equation may also be written as SST = SSM + SSE, where SS is notation for sum of squares and *T*, *M*, and *E* are notation for total, model, and error, respectively. The square of the sample correlation is equal to the ratio of the model sum of squares to the total sum of squares: $r^2 = \mathrm{SSM/SST}$. The interpretation of r^2 is to explain the fraction of variability in the data explained by the regression model. The sample variance s_y^2 is equal to:

$$s_y^2 = \frac{\sum_i (y_i - \bar{y})^2}{(n-1)}$$

Last equation is the total sum of squares divided by the total degrees of freedom (*df*). For simple linear regression, the MSM (mean square model) is given by:

$$\mathrm{MSM} = \sum_i (\hat{y}_i - \bar{y})^2 = \frac{\mathrm{SSM}}{\mathrm{DFM}}$$

The above is since the simple linear regression model has one explanatory variable *x*.

The corresponding MSE (mean square error) values are obtained by:

$$\mathrm{MSE} = \frac{\sum_i (y_i - \hat{y}_i)^2}{(n-2)} = \frac{\mathrm{SSE}}{\mathrm{DFE}}, \text{ respectively.}$$

3. Results and discussion

3.1. Limits of detection (LODs), smoothing procedure validation, accuracy, precision and assignment of the solid-state Raman spectra within THz-region

The solid-state Raman spectra of the studied compound **(1)**–**(5)** are depicted in Figs. 1 and 2. The spectroscopic patterns are

Table 5
Multiple regression analysis and ANOVA test the data in Table 1 for the $\nu_i^{(j)}$ and $A\nu_i^{(j)}$; the Prob. *F* value for all calculations is <0.0001.

Value	Std. Error	*t*-Value	Prob (>|*t*|)	r^2	ESD		*df*	SS	MS	*F* Statistic	
SG-L/R 2/2, PO = 2 vs. FFT/NP = 3											$\nu_i^{(j)}$
2.8×10^{-13}	2.4×10^{-9}	1.2×10^{-4}	0.9999_1	1	3.4×10^{-9}	Model	2	32102.1375	16051.0687_5	1.4×10^{-21}	
1	2.6×10^{-9}	3.8×10^{8}	<0.0001			Error	13	1.5×10^{-16}	1.5×10^{-17}		
2.1×10^{-12}	2.6×10^{-9}	7.9×10^{-9}	0.9993_8			Total	15	32102.1375			
SG-L/R 6/6, PO = 2 vs. FFT/NP = 5											
0.1696_4	0.0559_3	3.0328_1	0.0096_1	1	0.0745	Model	2	32102.03122	16051.0326_7	2.8×10^{-6}	
0.0506_7	0.064	0.7917_4	0.4427_2			Error	13	0.07216	0.00555		
0.9490_9	0.0638_7	14.860_2	<0.0001			Total	15	32102.1375			
SG-L/R 10/10, PO = 2 vs. FFT/NP = 7											
0.2036_4	0.0913_8	2.2286_5	0.0441_1	0.9999_9	0.1288	Model	2	32101.9218_4	16050.9609_2	967544.2193_7	
0.8144_7	0.1436_3	5.6704_9	<0.0001			Error	13	0.2156_6	0.0165_9		
0.1846_2	0.1437_2	1.2845_5	0.2213_7			Total	15	32102.1375			
SG-L/R 2/2, PO = 4 vs. FFT/NP = 3											
-1.2×10^{-12}	1.51513E−9	−7.74964E−4	0.99939	1	2.12335E−9	Model	2	32102.1375	16051.06875	3.6×10^{21}	
1	1.92856E−9	5.18523E8	<0.0001			Error	13	5.86122E−17	4.50863E−18		
1.4×10^{-12}	1.93209E−9	7.07475E−4	0.99945			Total	15	32102.1375			
SG-L/R 6/6, PO = 4 vs. FFT/NP = 5											
0.1315_2	0.06701	1.96255	0.07146	1	0.09042	Model	2	32102.03122	16051.0156_1	1.9×10^{6}	
-0.0274_3	0.08524	−0.32185	0.75268			Error	13	0.10628	0.0081_8		
1.0269	0.08506	12.0732	<0.0001			Total	15	32102.1375			
SG-L/R 10/10, PO = 4 vs. FFT/NP = 7											
0.2030_7	0.0994_2	2.0425_1	0.0619_3	0.9999_9	0.1363_2	Model	2	32101.8959_2	16050.9479_6	863735.2240_4	
0.9442_3	0.1956_7	4.8255_9	3.3×10^{-4}			Error	13	0.2415_8	0.0185_8		
0.0547_7	0.1958	0.2797_5	0.7840_7			Total	15	32102.1375			
SG-L/R 2/2, PO = 6 vs. FFT/NP = 3											
-1.3×10^{-12}	1.0×10^{-9}	-0.0012_7	0.9990_1	1	1.5×10^{-9}	Model	2	32102.1375	16051.0687_5	7.5×10^{21}	
1	1.3×10^{-9}	7.7×10^{8}	<0.0001			Error	13	2.8×10^{-17}	2.1×10^{-18}		
2.2×10^{-11}	1.3×10^{-9}	0.0169	0.9867_7			Total	15	32102.1375			
SG-L/R 2/2, PO = 6 vs. SG-L/R 2/2, PO = 4											
-2.6×10^{-12}	1.1×10^{-9}	-0.0024_3	0.9981	1	1.4×10^{-9}	Model	2	28507.8035_7	14253.9017_9	6.9×10^{21}	
1	1.4×10^{-9}	7.4×10^{8}	<0.0001			Error	11	2.3×10^{-17}	2.1×10^{-18}		
1.0×10^{-11}	1.4×10^{-9}	0.0074_2	0.9942_2			Total	13	28507.8035_7			
SG-L/R 6/6, PO = 6 vs. SG-L/R 6/6, PO = 4											
0.1335_1	0.0611_2	2.1842_8	0.0514_8	1	0.0832_7	Model	2	28507.7272_9	14253.8636_4	2.1×10^{6}	
0.0452_7	0.0699_7	0.6469_9	0.5309_1			Error	11	0.0762_8	0.0069_3		
0.9542	0.0697_5	13.6797_3	<0.0001			Total	13	28507.8035_7			
SG-L/R 10/10, PO = 6 vs. SG-L/R 10/10, PO = 4											
0.1777_5	0.0485_1	3.66392	0.00373	1	0.06681	Model	2	28507.7544_7	14253.8772_4	3.2×10^{6}	
0.9272_3	0.0812_6	11.41116	<0.0001			Error	11	0.0491	0.00446		
0.0724_5	0.081_{22}	0.89208	0.39145			Total	13	28507.8035_7			
SG-L/R 14/14, PO = 6 vs. SG-L/R 14/14, PO = 4											
0.1570_1	0.1136	1.3821_2	0.1902_2	0.9999_9	0.1601_1	Model	2	32101.8042_3	16050.9021_2	626109.4948	
0.4230_9	0.1431_5	2.9556_6	0.0111_5			Error	11	0.3332_7	0.0256_4		
0.5762_7	0.1430_9	4.0274_1	0.0014_4			Total	13	32102.1375			
SG-L/R 2/2, PO = 2 vs. FFT/NP = 3											$A\nu_i^{(j)}$
8.9×10^{-4}	0.0011_7	0.7544_7	0.4640_2	1	0.0025_3	Model	2	143.1172_2	71.5586_1	1.110^7	
1.0153_9	0.0042_4	239.2273_5	<0.0001			Error	13	8.310^{-5}	6.410^{-6}		
-0.0151_9	0.0043	-3.5291_2	0.0037			Total	15	143.1173_1			
SG-L/R 6/6, PO = 2 vs. FFT/NP = 5											
0.0446_6	0.0943_5	0.4733	0.6438_5	0.9968_2	0.1871_5	Model	2	142.6619_9	71.331	2036.6187_1	
0.4661_6	0.5798_1	0.8039_8	0.4358_6			Error	13	0.4553_1	0.0350_2		
0.5451_7	0.5723	0.9525_9	0.3581_7			Total	15	143.1173_1			
SG-L/R 10/10, PO = 2 vs. FFT/NP = 7											
0.0672_1	0.0861	0.7806_2	0.4490_1	0.9968_5	0.1861_6	Model	2	142.6667_7	71.3333_8	2058.2859_5	
-1.4667_1	1.3657_1	-1.0739_6	0.3023_7			Error	13	0.4505_4	0.0346_6		
2.4768_1	1.3694_3	1.8086_4	0.0936_8			Total	15	143.1173_1			
SG-L/R 14/14, PO = 2 vs. FFT/NP = 9											
0.0393_8	0.0748	0.5265	0.6074_1	0.9976_9	0.1594_6	Model	2	142.7867_5	71.3933_5	2807.7691_4	
3.6474_5	0.8506_3	4.2879_4	8.8×10^{-4}			Error	13	0.3305_5	0.0254_3		
-2.6461_1	0.8517_9	-3.1065_3	0.0083_4			Total	15	143.1173_1			
SG-L/R 2/2, PO = 4 vs. FFT/NP = 3											
2.9×10^{-4}	0.0011_8	0.2510_6	0.8056_9	1	0.0025_4	Model	2	143.1290_5	71.5645_3	1.1×10^{7}	
1.0159_1	0.0042	242.0207_6	<0.0001			Error	13	8.4×10^{-5}	6.5×10^{-6}		
-0.0156_8	0.0042_6	-3.6826_6	0.0027_6			Total	15	143.1291_4			
SG-L/R 6/6, PO = 4 vs. FFT/NP = 5											
0.0268	0.0932_8	0.2872_8	0.7784_3	0.9966_9	0.1908_5	Model	2	142.6556_5	71.3278_2	1958.3438_5	
0.6634_7	0.5795_7	1.1447_5	0.2729_5			Error	13	0.4734_9	0.0364_2		
0.3506_6	0.5725_2	0.6124_9	0.5507_8			Total	15	143.1291_4			
SG-L/R 10/10, PO = 4 vs. FFT/NP = 7											
0.0647_7	0.1054_8	0.6140_9	0.5497_5	0.9961_3	0.2064_1	Model	2	142.5752_9	71.2876_4	1673.2614_8	
-0.1467_2	2.2908	-0.0640_5	0.9499_1			Error	13	0.5538_5	0.0426		
1.1534	2.2975_8	0.5020_1	0.6240_6			Total	15	143.1291_4			

Table 5 (*Continued*)

Value	Std. Error	*t*-Value	Prob (>|*t*|)	r^2	ESD		*df*	SS	MS	*F* Statistic
SG-L/R 14/14, PO = 4 vs. FFT/NP = 9										
0.0648_2	0.0544_9	1.1896_9	0.2554_4	0.9987_2	0.1185_6	Model	2	142.9464_1	71.4732_1	5085.0052_9
4.0113_3	4.0113_3	7.0622_8	<0.0001			Error	13	0.1827_2	0.0140_6	
-3.0080_1	0.5682_8	-5.2931_6	1.5×10^{-5}			Total	15	143.1291_4		
SG-L/R 2/2, PO = 6 vs. FFT/NP = 3										
9.1×10^{-4}	0.0012_7	0.7129_1	0.4884	1	0.0027_5	Model	2	142.9633_4	71.4816_7	9.5×10^6
0.9849_7	0.0043_7	225.1492_4	<0.0001			Error	13	9.8×10^{-5}	7.6×10^{-6}	
0.0151_4	0.0044_3	3.4151_7	0.0046_1			Total	15	142.9634_3		
SG-L/R 6/6, PO = 6 vs. FFT/NP = 5										
-0.0429_2	0.0899_7	-0.4770_6	0.6412_4	0.9971_8	0.1761_2	Model	2	142.5602_1	71.2801	2298.0647_9
1.7489_5	0.5332_6	3.2797_4	0.0059_8			Error	13	0.4032_3	0.0310_2	
-0.7245	0.5282_1	-1.3716_2	0.1933_9			Total	15	142.9634_3		
SG-L/R 10/10, PO = 6 vs. FFT/NP = 7										
0.0907_7	0.0928_9	0.9772_3	0.3462_6	0.9962_7	0.2024_8	Model	2	142.4304_5	71.2152_3	1737.0225_6
1.6172_6	1.4603_6	1.1074_4	0.2881_7			Error	13	0.5329_8	0.041	
-0.6160_2	1.4638_3	-0.4208_3	0.6807_5			Total	15	142.9634_3		
SG-L/R 14/14, PO = 6 vs. FFT/NP = 9										
0.0640_7	0.064	1.0011_3	0.3350_3	0.9982_4	0.1390_5	Model	2	142.7120_8	71.3560_4	3690.4997_6
3.2543_6	0.5711_9	5.6975_3	<0.0001			Error	13	0.2513_6	0.0193_4	
-2.2566_1	0.5728_6	-3.9391_9	0.0017			Total	15	142.9634_3		
SG-L/R 2/2, PO = 2 vs. SG-L/R 2/2, PO = 6										
5.3×10^{-5}	9.5×10^{-4}	0.0560_5	0.9561_5	1	0.0020_6	Model	2	142.9633_8	71.4816_9	1.7×10^7
0.9706_9	0.0032_3	300.9413_5	<0.0001			Error	13	5.5×10^{-5}	4.2×10^{-6}	
0.0292_1	0.0032_7	8.9314_3	<0.0001			Total	15	142.9634_3		
SG-L/R 6/6, PO = 2 vs. SG-L/R 6/6, PO = 6										
-0.04681	0.0674_8	-0.6936_5	0.5001_1	0.9983_2	0.1359_6	Model	2	142.7231_3	71.3615_6	3860.5145_2
1.86449	0.3597_3	5.1829_8	1.8×10^{-4}			Error	13	0.2403	0.0184_8	
-0.84909	0.3583_4	-2.3695_3	0.0339_7			Total	15	142.9634_3		
SG-L/R 10/10, PO = 2 vs. SG-L/R 10/10, PO = 6										
0.0555_5	0.0716_9	0.7747_4	0.4523_5	0.9978_1	0.1552_1	Model	2	142.6502_8	71.3251_4	2960.9042_7
3.6434_2	1.0880_6	3.3485_5	0.0052_4			Error	13	0.3131_6	0.0240_9	
-2.6409_8	1.0889	-2.4253_8	0.0305_9			Total	15	142.9634_3		
SG-L/R 14/14, PO = 2 vs. SG-L/R 14/14, PO = 6										
0.0458_1	0.0578_4	0.7921_3	0.4425	0.9985_8	0.1248_8	Model	2	142.7606_7	71.3803_4	4576.4859_2
2.6792_3	0.4068_8	6.5845_8	<0.0001			Error	13	0.2027_7	0.0156	
-1.6779_5	0.4078_4	-4.1142_5	0.0012_2			Total	15	142.9634_3		
SG-L/R 2/2, PO = 4 vs. SG-L/R 2/2, PO = 6										
6.7×10^{-4}	0.0010_3	0.6483_4	0.5280_5	1	0.0022_1	Model	2	142.9633_7	71.4816_9	1.5×10^7
0.9702_9	0.0034_7	279.6633_3	<0.0001			Error	13	6.4×10^{-5}	4.9×10^{-6}	
0.0295_8	0.0035_2	8.4069_3	<0.0001			Total	15	142.9634_3		
SG-L/R 6/6, PO = 4 vs. SG-L/R 6/6, PO = 6										
-0.0685_9	0.0650_8	-1.0539_4	0.3111	0.9985	0.1284_6	Model	2	142.7489	71.3744_5	4325.0112_3
2.1101	0.3750_6	5.6259_7	<0.0001			Error	13	0.2145_4	40.0165	
-1.0928	0.3734_3	-2.9264_1	0.0117_9			Total	15	142.9634_3		
SG-L/R 10/10, PO = 4 vs. SG-L/R 10/10, PO = 6										
0.0083_6	0.0865_6	0.0965_5	0.9245_5	0.9972	0.1756_4	Model	2	142.5624_5	71.2812_3	2310.9692_2
3.6489_1	1.5010_1	2.4309_7	0.0302_8			Error	13	0.4009_8	0.0308_4	
-2.6436_9	1.5009_8	-1.7613	0.1016_7			Total	15	142.9634_3		
SG-L/R 14/14, PO = 4 vs. SG-L/R 14/14, PO = 6										
-0.0114_7	0.0549_6	-0.2086_7	0.8379_4	0.9988	0.1149_1	Model	2	142.7917_8	71.3958_9	5407.0922
3.4724_9	0.4744_4	7.3192	<0.0001			Error	13	0.1716_5	0.0132	
-2.4723_7	0.4754_2	-5.2003_9	1.7×10^{-4}			Total	15	142.9634_3		

ESD: estimated standard deviation; *df*: degrees of freedom; SS: sum of squares; MS: mean squares.

validated, using *one* component system. The optimization starts by standard smoothing procedure, including the SG and FFT methods. The polynomial order varied within two–six. The number of points from left and right (L/R) side of the curve are within 2/2–22/22 (SG method) and from 2 to 9 for FFT method, respectively. The observed frequencies within the 200–30 cm^{-1} region are summarized in Tables 1 and 2, respectively. The results for $\nu_i^{(j)}$ and $A\nu_i^{(j)}$ are analysed by Student's *t*-test (Table 3). The obtained *p* values are within 0.007–0.0001 by Fourier (FFT) smoothing (NP 3 and 5) method. *P* = 0.36 is obtained at FFT and NP = 9. The corresponding *p* values by SG method and polynomial order 2 at L/R within 2/2–18/18 are within 0.052–0.0004, respectively. The calculated *p*- and *t*-data (Table 3) are compared with tabulated data at 99% confidence level, so as to verify the absence of statistically significant differences. The data clearly show that the application of the individual function to the different complicated spectroscopic patters appear suitable for such spectroscopic analysis. It must be noted that the polynomial order weakly effects to the obtained peak positions and the integral intensities (Fig. 2, Table 3). In contrast the increasing of the number of points L/R leads to the decreasing of the obtained $A\nu_i^{(j)}$ and $A\nu_i^{(j,k)}$ values. Moreover are obtained different dependences for the determination of the $A\nu_i^{(j)}$ and ν_i (Table 5, Fig. 5). These results assumes that for here analysed systems, the best correlation between original patterns and smoothed curves are obtained using FFT method with number of points 3 or SG method at polynomial order 2 and L/R 2/2–10/10, respectively. The accuracy, repeatability and precision are also shown in the Table 1.

The frequency assignment (Table 2) is based on the obtained crystallographic data. Typical for all **(1)–(5)** systems is the observed H-bond deformations (Scheme 1) within 180–111 cm^{-1} (5.4–3.3 THz). The corresponding skeletal modes are found within 103–60 cm^{-1} (3.1–1.8 THz). The torsion mode in of entire side chain about the aromatic system in **(5)** is observed at 55 cm^{-1} (1.7 THz), respectively. The first group of peaks are characterized

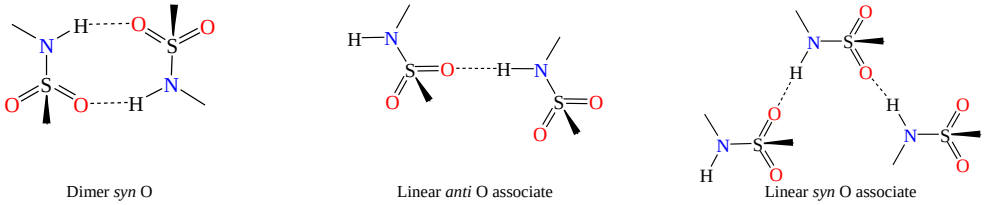

Scheme 1. Dimer and linear hydrogen bond associates of the sulfonamide group and the chain motif formed with *anti* and *syn* O acceptor atoms.

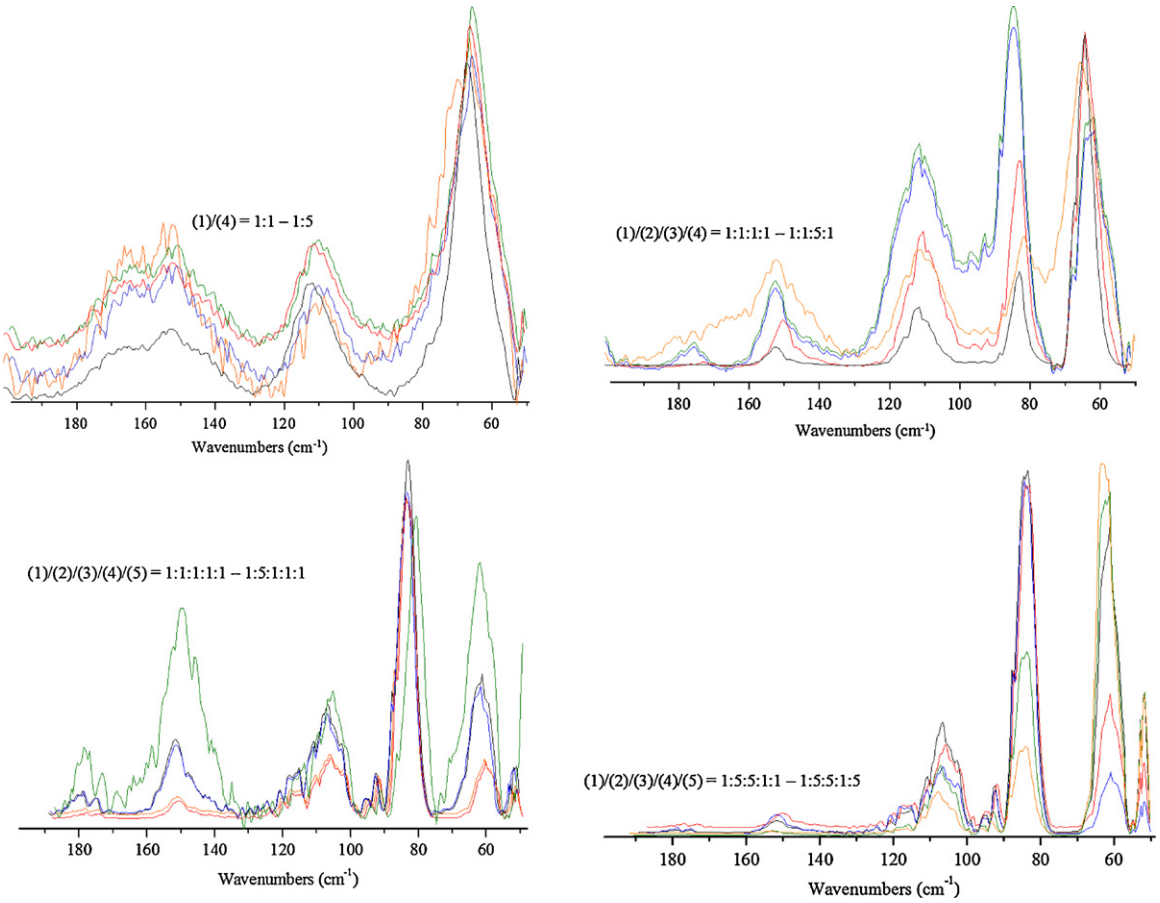

Fig. 3. Solid-state Raman spectras of the binary and *n*-component mixtures at different molar ratios.

with a broad character, and relatively low-intensity. In contrast, the corresponding skeletal vibrations are characterized with relatively sharp profile, thus making this group of frequencies as most appropriated for the quantitative determination. On the other side, the observed overlapping effects within the region of 3.1–1.8 THz, difficult the quantitative analysis by the isolated mode, characteristic for each of the studied compounds. For the identification of the solid (including crystalline) materials, the strong individual profile of the spectroscopic patterns within THz-region, allows unambiguously determination of the chemicals, depending of the type of hydrogen bonds, the space system for the crystals, the number of the molecules per unit cell and more. In the case of **(5)**, the complex character of the Raman patters is result of the presence of both types of intermolecular hydrogen bonds, *anti* and *syn* O (Scheme 1) [51]. In such cases the individual approach for mathematical interpretation of the observed frequencies appears obligatory strongly depending of the intensity of the excitations, level of overlapping effect, broad profile of the curves and more. Similar to the quantitative analysis within *mid*-IR region by IR- and Raman spectroscopy [23–31], the strong intensive and well defined non-overlapped peaks result to the lower *LODs* values. For the quantitative analysis of **(4)** and **(5)** in the mixtures with (**1**) and (**3**), the best *LODs* values are obtained, using the strong intensive peaks at 72 cm^{-1} and 55 cm^{-1}, respectively. The $Av_i^{(j,k)}$ are obtained, using the excitations of the H-bond deformations. Independently of their relatively low intensities, the well defines characterized and low-level of overlapping effect result to the lowest achieved data for *LODs*.

The excitations used for the quantitative determinations of the different mixtures are: ***(1)***/***(4)***: ν_1 = 60 ± 0.1 cm^{-1}, ν_2 = 72 ± 0.1 cm^{-1} (**1**); ***(2)***/***(5)***: ν_1 = 153 ± 0.2 cm^{-1}, ν_2 = 55 ± 0.4 cm^{-1} (**5**); ***(3)***/***(4)***: ν_1 = 157 ± 0.3 cm^{-1}, ν_2 = 72 ± 0.4 cm^{-1} (**3**); ***(2)***/***(3)***/***(4)***: ν_1 = 62 ± 0.3 cm^{-1}, ν_2 = 72 ± 0.4 cm^{-1} (**3**) and ν_2 = 144 ± 0.2 cm^{-1} (**4**); ***(1)***/***(3)***/***(4)***/***(5)***: ν_1 = 62 ± 0.3 cm^{-1}, ν_2 = 85 ± 0.2 cm^{-1} (**3**); ***(1)***/***(2)***/***(3)***/***(4)***: ν_1 = 62 ± 0.3 cm^{-1}, ν_2 = 83 ± 0.2 cm^{-1} (**2**)/(**3**); ***(1)***/***(2)***/***(3)***/***(4)***/***(5)***: ν_1 = 62 ± 0.3 cm^{-1}, ν_2 = 83 ± 0.2 cm^{-1} (**2**)/(**3**); ***(1)***/***(2)***/***(3)***/***(4)***/***(5)***: ν_1 = 73 ± 0.3 cm^{-1}, ν_2 = 55 ± 0.4 cm^{-1} (**5**). The obtained patterns of the individual drugs and the mixtures (Figs. 2 and 4) are procedure by the non-linear curve-fitting method, using the

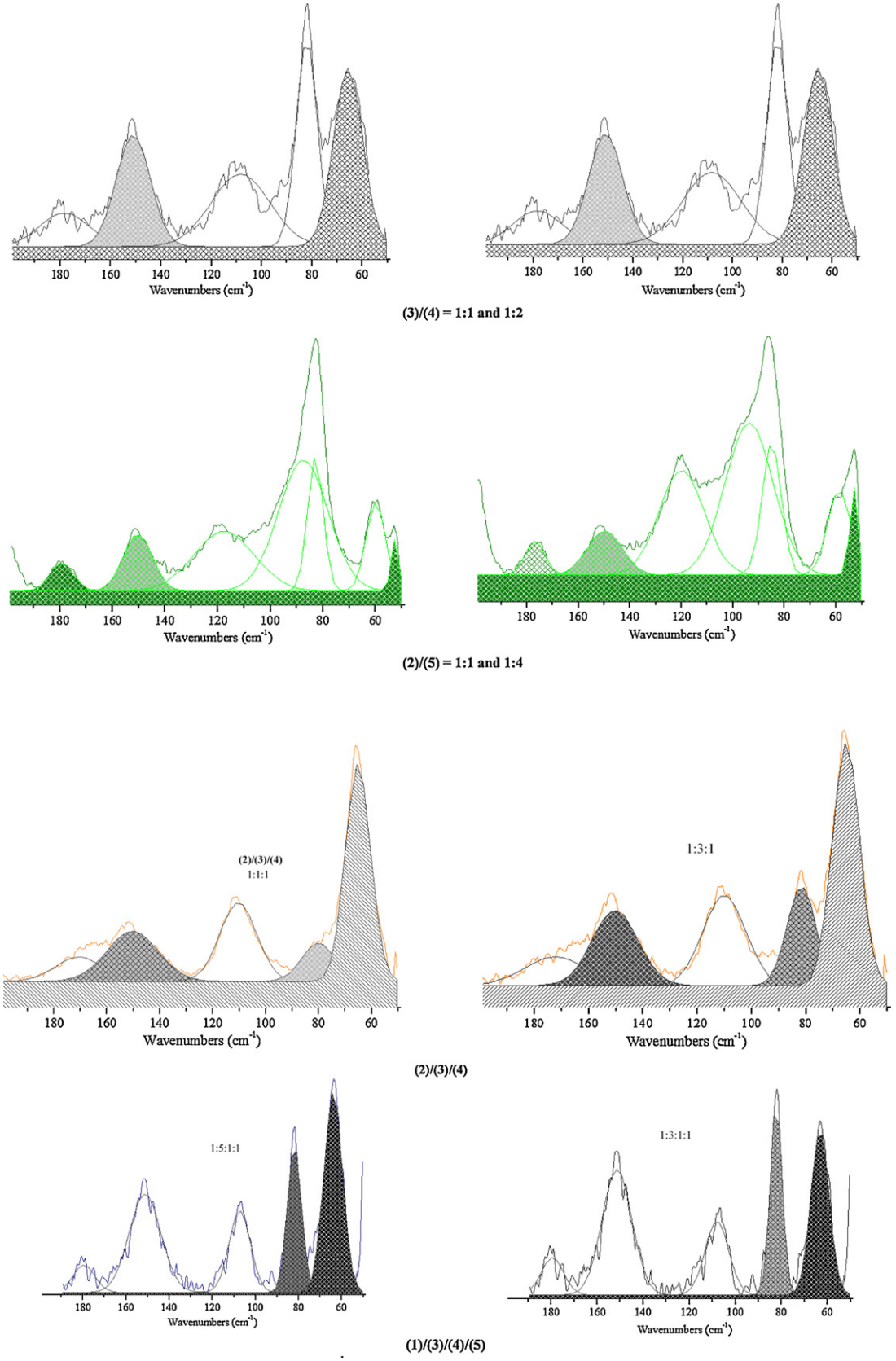

Fig. 4. Curve-fitted solid-state Raman spectra within the 200–30 cm^{-1} of the solid mixtures of compounds studied at different molar ratios; curve-fitted spectroscopic patterns after the baseline correction method, by non-linear multipeak Lorenzian–Gaussian function at ratio 1:1; *A* is the total area under the curve from the baseline centre of the peak; w^2 "sigma", approximately 0.441 the FWHM; $w/2$ is the standard deviation, respectively.

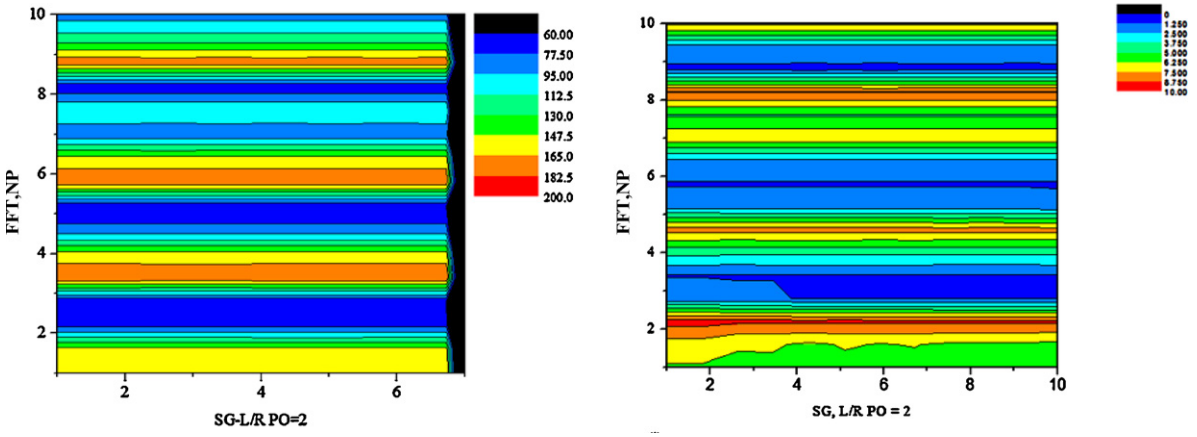

Fig. 5. 2D image plot of the statistical correlations between the methods towards the $\nu_i^{(j)}$ and $A\nu_i^{(j)}$ values.

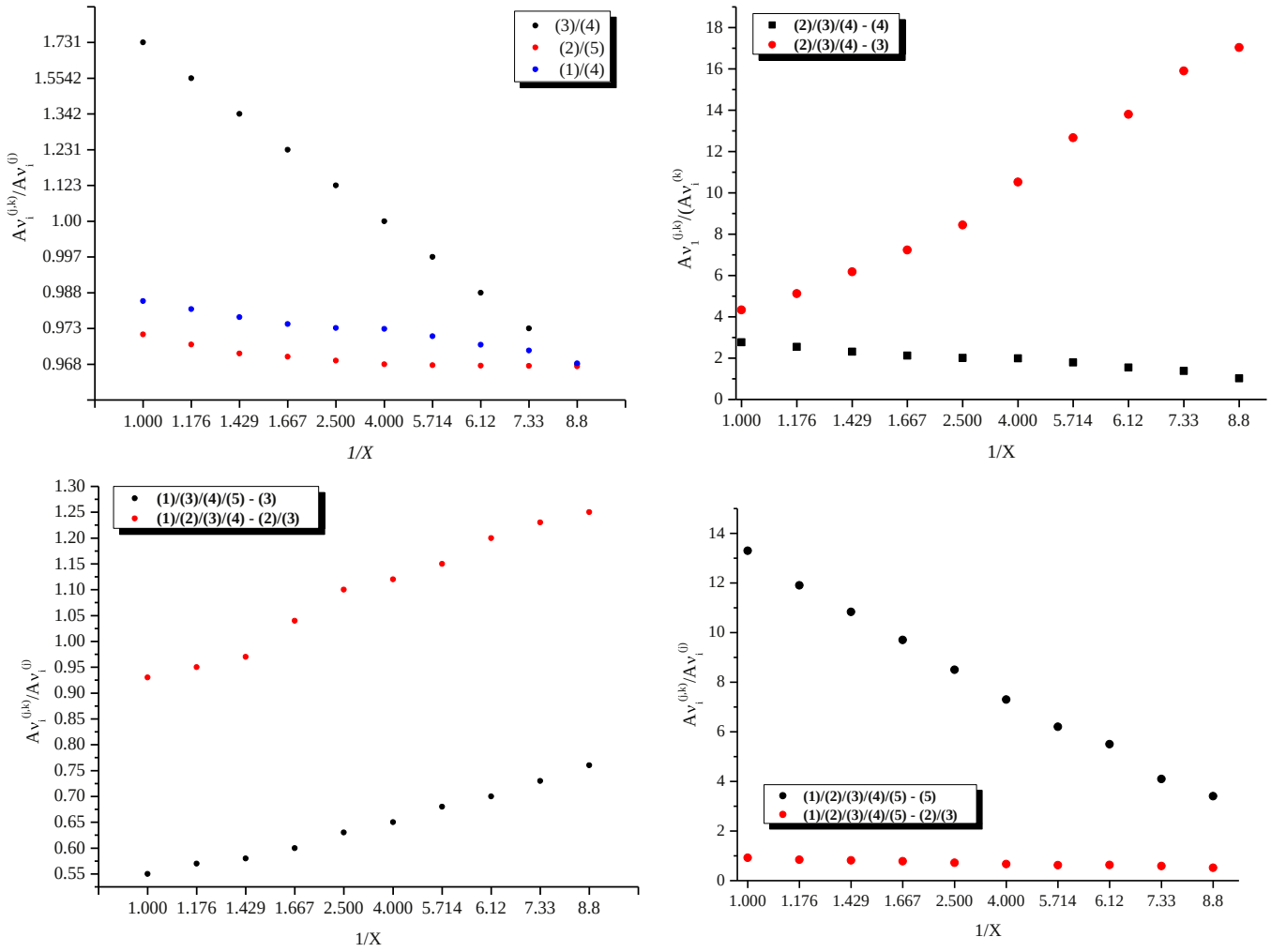

Fig. 6. The straight-line plot from the regression analysis of the *n*-component mixtures.

Lorenzian-Gaussian mixed [23–32] functions at ratio 1:1 at 2000–4000 iterations. The obtained *p* values around 0.0042 indicate difference between means at 99% and below the critical value of 0.05. Regression analysis (Fig. 7) of the data gave a straight-line calibration plots (Table 4). The obtained *LODs* for **(2)**/**(3)** are 0.010 mole fraction. This result indicates, unambiguously the capability and perspectives in front the quantitative analysis within THz-region. The relatively high *LODs* value for 0.072 for the analysis of **(1)** in system **(1)/(4)** is explain with the complicated individual spectroscopic patterns of the compounds, characterizing with the broad and relatively overlapped frequencies (Fig. 3). For the *n*-component mixtures with $n = 3$–5, the obtained data depends strongly of the chosen mode. As can be seen (Table 4, Figs. 3 and 4) the dependence of $A\nu_i^{(j\ldots n)}/A\nu_i^{(j)}$ vs. the mole fraction of the determining substances, result to r^2 values within 0.9984_4–0.9884_3, respectively. Comparing the highest obtained value for the $n = 5$

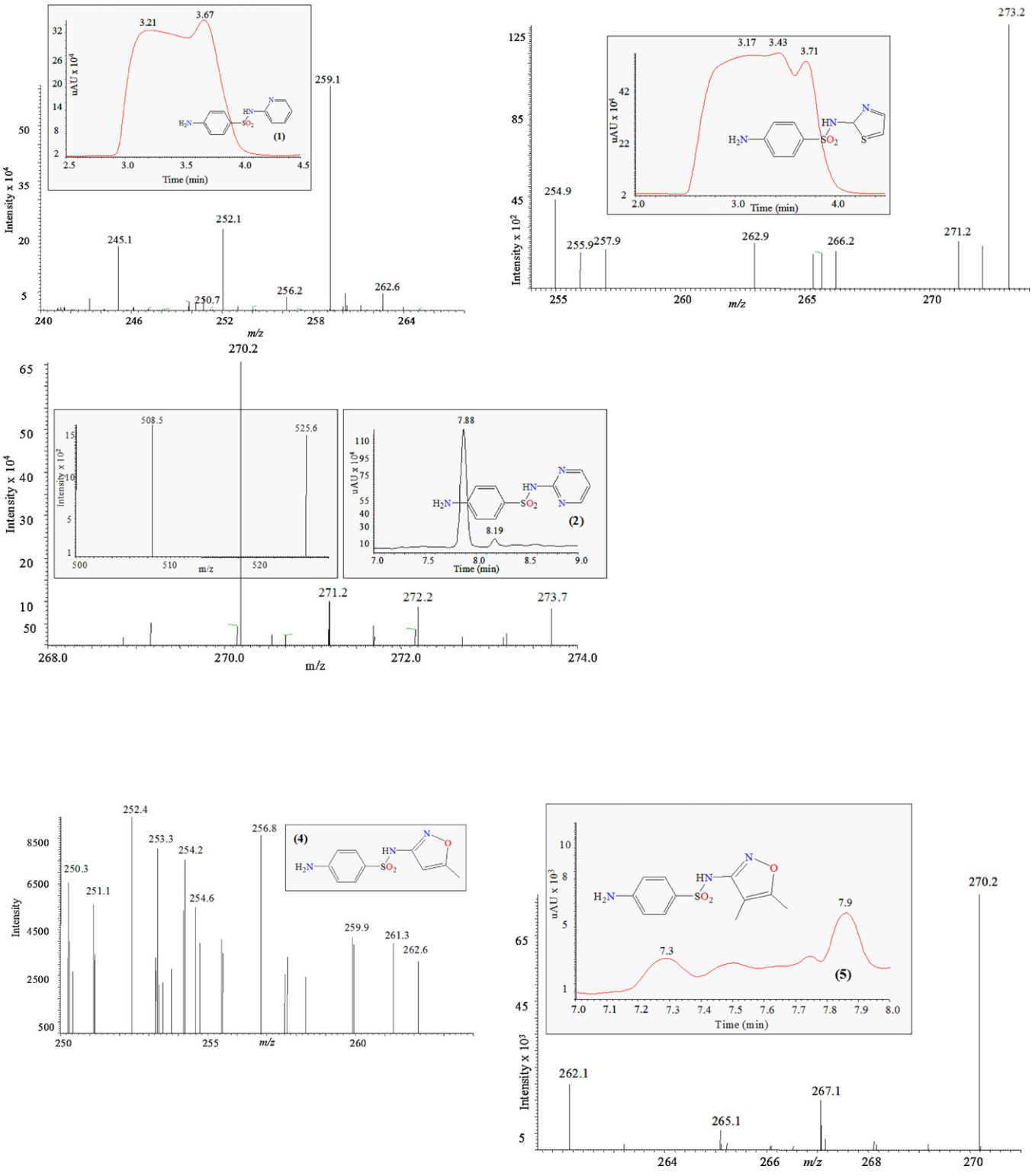

Fig. 7. HR HPLC ESI-MS/MS data of (**1**)–(**5**), respectively.

(*i.e.* system **(1)/(2)/(3)/(4)/(5)**, towards the determination of **(5)**) and this for $n = 2$ (**(3)/(4)**, analysing the **(3)**), only a decreasing of the 0.1_5% is obtained. This result in addition illustrates the great capability of the method for detection of multicomponent mixtures. It should however taking into account that the spectroscopic patterns of the mixtures for the system $n = 5$ (**(1)/(2)/(3)/(4)/(5)**) are characterized with the strong intensive frequencies and low degree of overlapping effect. It is interesting to note as well that the analysis of the systems $n = 4$ (**(1)/(2)/(3)/(4)–(3)/(2))** and $n = 5$ **((1)/(2)/(3)/(4)/(5)–(3)/(2))** results to the reliable data for r^2 of 0.9917_5 of 0.9884_3, respectively. The observed overlapping effect of corresponding excitations of the skeletal modes and the torsion of entire side chain about the aromatic system result to the determination of the compounds **(2)/(3)** as sum. In this case, the obtained relatively lower value of r^2, is explain additionally with the shifting effect of the used for the quantitative analysis excitations at

about $\pm 3\,cm^{-1}$. Such effect result to the increasing of the error of the used mathematical methods for determination of the ν_i, respectively. The demonstrate, sensitivity of the obtained quantities using the vibrations within THz-region must be done carefully taking into account as well the factor, signal to noise (S/N). Such for example, systems (**1**)/(**4**) (Fig. 1) and (**1**)/(**2**)/(**3**)/(**4**)/(**5**) (Fig. 4) are characterized with low S/N ratio, thus resulting to application of the FFT and SG methods ate relatively high polynomial order and NP. As can be seen from the obtained r^2 values the error effect significantly influenced the $A\nu_i$ values at about 0.14%, both applying the non-linear and MLR methods (below). The obtained parallel data from the multiple linear regression and ANOVA test for MLR are summarized in Table 5 and visualized in Fig. 5, respectively. The obtained r^2 values within the 0.9999_8–0.9988_6, especially determining the $A\nu_i$ values, prove additionally that there is no one perfect one mathematical method to fit the experimental data-set. As obtained for example to the obtained r^2 value by the non-linear peak fitting methods of 0.9998_9 for determining the $A\nu_I$, corresponds a 0.9968_6 by the MLR method. The obtained difference of the 0.3%, indicate dominantly the application of individual functional simulations.

3.2. HPLC tandem ESI-MS/MS mass spectrometry

The correlations between the results in samples with different amounts of (**1**)–(**5**) for all of studied systems, obtained by spectroscopic Raman and HPLC ESI MS/MS technique demonstrate good agreement with correlation coefficients > 0.9998. HPLC ESI MS/MS analyses of the isolated compounds were performed using the procedures described [31] for quantitative determination. The corresponding m/z values of each of the samples in the isolated components as well as at the binary mixtures are shown in the same figure as well as the relatively abundance times in corresponding chromatograms. The observed peaks m/z at 259.1, 263.8, 264.2, 262.6, 270.2 correspond to the cations of the **(1)**–**(5)**, *i.e.* $[C_{11}H_{12}N_3SO_2]^+$, $[C_{10}H_{11}N_4SO_2]^+$, $[C_9H_9N_3S_2O_2]^+$, $[C_{10}H_{11}N_3SO_3]^+$ and $[C_{11}H_{14}N_3SO_3]^+$ with the molecular weights of 259.1, 262.8, 264.3, 262.8, and 270.9 respectively. The corresponding values in the binary mixtures are weak effects. Only in the systems **(1)** and **(2)**, the observed peaks at higher values of m/z 518.4 and 525.6 which could assigned to the stable associates in gas phase [57,58], most probably related to the typical for pyridinium systems $N_{(Py)}\cdots H\cdots N$-dimers (Figs. 6 and 7).

4. Conclusions and outlook

In this paper, we have outlined the possibilities of the vibrational analysis within the THz-region towards the quantitative elucidation, determination and identification of the individual drugs and solid n-component mixtures. The solid-state Raman spectroscopy and the non-linear mathematical methods for interpretation of the spectroscopic patterns result to low *LODs*. Perhaps most importantly, it is essential to nightlight the new perspectives in front IR-, Raman and THz-spectroscopy within THz-region for complete assignment of the optical phenomena, unambiguous materials identification in solid-state [1–21]. The advantages for non-destructive materials identification and application in the interdisciplinary technological fields such as development of methods for security, environmental inspection, detection and protection are towards both qualitative and quantitative analysis. The results, demonstrated as well, the advantages of the solid-state Raman spectroscopy, using the excitations of H-bond deformations, skeletal modes, and/or lattice vibrations within THz-region, and the application of the additional mathematical methods for spectroscopic curve procedure, resulting to low *LODs*. Especially for the analysis of the complex patterns of n-component solid mixtures is shown remarkable for the vibrational spectroscopy *LODs* of the Raman spectroscopy 1.34%. The analysis of the five model systems of the sulfonamide drugs as isolated chemicals and in the n-component mixtures, show *LODs* within 0.010–0.012 mole. The dependences of integral area under the curves $AP^{(j\cdots n)}/AP^{(j)}$ vs. the mole fraction of the determining substances result to regression factor r^2 0.9984_4–0.9884_3 for $n = 5$ and 0.9998_9 for $n = 2$, respectively. It should taking into account that the application of the THz-spectroscopic range, for analysis requires an individual functional approach for elucidation and characterization. Thus, the performed parallel to the non-linear approach, the multiple linear regression analysis show r^2 values 0.9999_8–0.9988_6, respectively. The highest one is obtained determining the ν_i of binary mixture, respectively. The analysis of the AP, however using the non-linear methods results to better factor (0.9998_9) about 0.14% for tricomponent solid mixture. These results, illustrate the large potential for further investigations of the solid-mixtures towards validation and defining of the advantages and limitations of the analysis within THz-region for identification and especially for quantitative determination.

Acknowledgements

The authors thank the Deutscher Akademischer Austausch Dienst (DAAD), for a grant within the priority program "Stability Pact South-Eastern Europe" and the Deutsche Forschungsgemeinschaft (DFG) for Grants SPP 255/21-1 and SPP/22-1. The authors also thank the central instrumental laboratories for structural analysis at Dortmund University of Technology (Germany) and the analytical and computational laboratories at the Institute of Environmental Research (INFU) at the TU Dortmund (Germany).

References

[1] X. Zhang, Phys. Med. Biol. 47 (2002) 3667–3677.
[2] K. Siebert, K. Löffler, H. Quast, M. Thomson, T. Bauer, R. Leonhardt, S. Czasch, H. Roskos, Phys. Med. Biol. 47 (2002) 3743–3748.
[3] M. van Exter, D. Grischkowsky, IEEE Trans. Microwave Theory Technol. 38 (1990) 1684–1691.
[4] J. Kindt, C. Schmuttenmaer, J. Phys. Chem. 100 (1996) 10373–11379.
[5] M. van Exter, C. Fattinger, D. Grischkowsky, Opt. Lett. 14 (1989) 1128–1130.
[6] D. Mittleman, R. Jacobsen, M. Nuss, IEEE J. Sel. Top. Quantum. Electron. 2 (1996) 679–692.
[7] P. Günter, Nonlinear Optical Effects and Materials, vol. 72, Springer, 2000.
[8] P. Siegel, IEEE Trans. Microwave Theory Technol. 50 (2002) 910–928.
[9] R. Lewis, Proc. IEEE 95 (1995) 1641–1650.
[10] C. Weiss, R. Wallenstein, R. Beigang, Appl. Phys. Lett. 77 (2000) 4160–4162.
[11] B. Ferguson, X-C. Zhang, Nat. Mater. 1 (2002) 26–33.
[12] M. Tonouchi, Nat. Photonics 1 (2007) 97–105.
[13] C. Jansen, S. Wietzke, O. Peters, M. Scheller, N. Vieweg, M. Salhi, N. Krumbholz, C. Jördens, T. Hochrein, M. Koch, Appl. Opt. 49 (2010) E48–E57.
[14] D. Mittleman, Sensing with Terahertz Radiation, Springer-Verlag, 2003.
[15] M. Herrmann, M. Tani, K. Sakai, Jpn. J. Appl. Phys. 39 (2000) 6254–6258.
[16] S. Wietzke, C. Jansen, F. Rutz, D. Mittleman, M. Koch, Polym. Test. 26 (2007) 614–618.
[17] C. Jördens, M. Scheller, S. Wietzke, D. Romeike, D. Jansen, T. Zentgraf, K. Wiesauer, V. Reisecker, M. Koch, Compos. Sci. Technol. 70 (2010) 472–477.
[18] P. Kim, J. Jeong, M. Jazbinsek, S. Kwon, H. Yun, J. Kim, Y. Lee, I. Baek, F. Rotermund, P. Günter, O. Kwon, CrystEngComm 13 (2011) 444–451.
[19] B. Ruiz, Z. Yang, V. Gramlich, M. Jazbinsek, P. Günter, J. Mater. Chem. 16 (2006) 2839–2842.
[20] M. Koch, Proc. SPIE-Conf., 1999.
[21] M. Theuer, R. Beigang, D. Grischkowsky, Appl. Phys. Lett. 96 (2010) 191110.
[22] A. Redo-Sanchez, G. Salvatella, R. Galceran, L. Roldos, J. Garcia-Reguero, M. Castellari, J. Tejada, Analyst 136 (2011) 1733–1768.
[23] B. Ivanova, D. Tsalev, M. Arnaudov, Talanta 69 (2006) 822–828.
[24] B. Ivanova, V. Simeonov, M. Arnaudov, D. Tsalev, Spectrochim. Acta 67 (2007) 66–75.
[25] B. Ivanova, J. Mol. Struct. 738 (2005) 233–238.
[26] B. Koleva, T. Kolev, V. Simeonov, T. Spassov, M. Spiteller, J. Incl. Phenom. 61 (2008) 319–333.
[27] B. Koleva, J. Mol. Struct. 800 (2006) 23–27.
[28] B. Koleva, T. Kolev, D.L. Tsalev, M. Spiteller, J. Pharm. Biomed. Anal. 46 (2008) 267–273.
[29] B. Koleva, T. Kolev, M. Spiteller, J. Pharm. Biomed. Anal. 48 (2008) 201–204.

[30] J. Al-Zoubi, S. Koundourellis, S. Malamataris, J. Pharm. Biomed. Anal. 29 (2002) 459–467.
[31] T. Pfeifer, J. Tuerk, K. Bester, M. Spiteller, Rapid Comm. Mass Spectrom. 16 (2002) 663–669.
[32] http://de.openoffice.org/.
[33] C. Kelley, SIAM Front. Appl. Math. (1999) 18–27.
[34] K. Madsen, H. Nielsen, O. Tingleff, Informatics and Mathematical Modelling, 2nd ed., DTU Press, 2004.
[35] P. Stephens, D. McCann, J. Cheeseman, M. Frisch, Chirality 17 (2005) S52–S54.
[36] P. Stephens, F. Devlin, J. Cheeseman, M. Frisch, O. Bortolini, P. Besse, Chirality 15 (2005) S57–S64.
[37] A. Yildiz, P. Selvin, Accts. Chem. Res. 38 (2005) 574–585.
[38] D. Marquardt, J. Soc. Ind. Appl. Math. 11 (1963) 431–441.
[39] S. Savitzky, M. Golay, Anal. Chem. 36 (1964) 1627–1639.
[40] G. Steiner, Anal. Chem. 44 (1972) 1906–1909.
[41] M. Madden, Anal. Chem. 50 (1978) 1383–1386.
[42] C. Brown, P. Lynch, R. Obremski, D. Lavery, Anal. Chem. 54 (1982) 1472–1479.
[43] D. Haaland, R. Easterling, Appl. Spectrosc. 34 (1980) 539–546.
[44] H. Haaland, R. Easterling, Appl. Spectrosc. 36 (1982) 665–672.
[45] D. Haaland, R. Easterling, D. Vopicka, Appl. Spectrosc. 39 (1985) 73–84.
[46] P. Griffiths, G. Pariente, TrAC Trends Anal. Chem. 5 (1986) 205–209.
[47] K. Lindberg, A. Wägner, Acta Crystallogr. B33 (1997) 2165–2172.
[48] M. Ashraf-Khorassani, L. Taylor, L. Koeth, A. Roush, J. Chromatogr. B 1033 (2004) 221–224.
[49] C. Fagerquist, A. Lightfield, S. Lehotay, J. Anal. Chem. 77 (2005) 1473–1482.
[50] B. Ivanova, M. Spiteller, Biopolymers 39 (2010) 727–734.
[51] P. Sanphui, B. Sarma, A. Nangia, Cryst. Growth Des. 10 (2010) 4550–4564.
[52] D. Kleinbaum, Applied Regression Analysis and Other Multivariable Methods, 4th ed., Brooks/Cole, Belmont, Australia, CA, 2008.
[53] S. Wold, in: H. van de Waterbeemd (Ed.), PLS for Multivariate Linear Modeling QSAR: Chemometric Methods in Molecular Design. Methods and Principles in Medicinal Chemistry, Verlag-Chemie, 1994.
[54] L. Fahrmeir, G. Tutz, Multivariate Statistical Modelling Based on Generalized Linear Models, Springer-Verlag, New York, 1994.
[55] K.E. Muller, Bethel A. Fetterman, Regression and ANOVA, An Integrated Approach Using SAS Software, John Wiley & Sons Inc., 2003.
[56] T. Richter, Discourse Process. 41 (2006) 221–250.
[57] M. Lamshöft, B. Ivanova, J. Coord. Chem. 64 (2011) 2419–3264.
[58] M. Lamshoft, J. Storp, B. Ivanova, M. Spiteller, Polyhedron (2011), doi:10.1016/j.poly.2011.07.003.